

DIPLOMA THESIS

Feng Yuan
2024

HUNGARIAN UNIVERSITY OF AGRICULTURE AND LIFE SCIENCES
INSTITUTE OF LANDSCAPE ARCHITECTURE, URBAN PLANNING AND GARDEN ART
BUDAPEST

MASTER OF ARTS IN LANDSCAPE ARCHITECTURE AND GARDEN ART

**CHANGES IN CARBON SEQUESTRATION CAPACITY OF URBAN GREEN
SPACES AND OPTIMIZATION PATHWAYS: A CASE STUDY OF ZHENGZHOU
METROPOLITAN AREA**

FENG YUAN

JOMBACH SÁNDOR

BUDAPEST, 2024

Contents

| | |
|-------------------------------------------------------------------------------------|----|
| Abstract | 5 |
| 1. Introduction..... | 7 |
| 1.1. Research background | 7 |
| 1.1.1. Disruption of terrestrial carbon cycle | 7 |
| 1.1.2. Significant carbon sequestration in urban green spaces..... | 8 |
| 1.1.3. Difficulties faced by China..... | 9 |
| 1.2. Relative concept | 10 |
| 1.2.1. Carbon sequestration | 10 |
| 1.2.2. Urban green space..... | 11 |
| 1.3. International research progress..... | 12 |
| 1.3.1. Bibliometric analysis in the field of carbon sinks in urban green spaces.... | 12 |
| 1.3.2. Methodology for estimating carbon sequestration in urban green spaces | 16 |
| 1.4. Research content..... | 20 |
| 1.5. Research proposal | 20 |
| 1.6. Technological route | 20 |
| 2. Materials and Methods | 22 |
| 2.1. Research area | 22 |
| 2.2. Extract the main built area of cities..... | 26 |
| 2.3. Sample point setting and field survey..... | 28 |
| 2.3.1. Set plots for field research | 28 |
| 2.3.2. Field research | 29 |
| 2.4. Remote sensing image data..... | 32 |
| 2.4.1. Land use and land cover data | 32 |
| 2.4.2. Normalized Difference Vegetation Index (NDVI) | 36 |
| 2.5. Quantification of carbon sequestration..... | 37 |
| 2.5.1. Calculation of carbon sequestration capacity of trees | 37 |

| | | |
|--------|-------------------------------------------------------------------------------------------------------------------|----|
| 2.5.2. | Calculation of carbon sequestration capacity of shrubs | 37 |
| 2.5.3. | Calculation of carbon sequestration capacity of ground cover | 39 |
| 2.5.4. | Calculation of carbon sequestration capacity of urban green space..... | 40 |
| 2.6. | Landscape pattern | 43 |
| 2.7. | Boosted Regression Trees model | 45 |
| 3. | Result..... | 46 |
| 3.1. | Spatial-temporal dynamics of carbon sequestration in the main urban area of the Zhengzhou metropolitan area | 47 |
| 3.1.1. | General spatial-temporal dynamics of carbon sequestration | 47 |
| 3.1.2. | Spatial-temporal dynamics of carbon sequestration between cities | 48 |
| 3.2. | Characteristics of spatio-temporal differentiation of landscape pattern | 53 |
| 3.3. | Correlation analysis between landscape pattern and urban carbon sequestration | 55 |
| 3.4. | Relative contribution of landscape pattern indices to carbon sequestration..... | 57 |
| 4. | Discussion | 58 |
| 4.1. | Carbon sequestration changes in urban green spaces..... | 59 |
| 4.2. | Landscape drivers of carbon sequestration capacity in urban green spaces | 60 |
| 4.3. | Regulatory strategies based on carbon sinks in urban green spaces. | 61 |
| 5. | Conclusion | 63 |
| 5.1. | Research Results..... | 64 |
| 5.2. | Research Shortcomings | 64 |
| 5.3. | Research Prospects..... | 65 |
| | Reference | 66 |
| | Appendix | 75 |

Abstract

The terrestrial carbon cycle is always in a dynamic equilibrium, its importance is self-evident.

It concerns many aspects closely related to human well-being, ecosystem services, food security, timber production, and so forth. On one hand, the respiration of animals and plants, energy consumption, and other pathways release carbon stored in the soil and bodies of animals and plants into the atmosphere. Meanwhile, plants re-store carbon elements from the atmosphere into vegetation and soil carbon pools through processes like photosynthesis, achieving dynamic balance. Cities are the main areas of carbon emissions. With the continuous deepening of urbanization, urban green space systems are constantly being destroyed, and land types are being converted into construction land. **The terrestrial carbon cycle is disrupted.**

This paper takes the Zhengzhou metropolitan area in China as an example and, based on promoting the carbon sequestration of urban green spaces, explores the correlation between urban green space carbon sequestration and multiple landscape indices by combining field survey data with remote sensing image data, aiming to explore the optimal urban planning model and provide theoretical references for urban planning and the layout of urban green space systems.

The research results show:

- Over a period of 10 years from 2013 to 2023, with 5-year intervals, the carbon storage in the Zhengzhou metropolitan area showed an overall increasing trend, with an **average annual growth rate of 0.018 Kg C/m² yr.**
- Among the nine cities within the Zhengzhou metropolitan area, **Kaifeng consistently ranked first in urban green space carbon sequestration over 10 years**, showing positive growth trends. In 2023, the urban green space carbon sequestration in Kaifeng reached 0.942 Kg C/m² yr.
- The carbon sequestration of urban green spaces in the Zhengzhou metropolitan area is significantly positively correlated with landscape indices such as Contrast-weighted Edge Density (CWED), Shannon's Evenness Index (SHEI), and Splitting Index (SPLIT), and

significantly negatively correlated with indices such as Mean of Perimeter-Area Ratio (PARA_MN), Number of patches (NP), Mean patch area (AREA_MN), Percentage of Like Adjacencies (PLADJ), and Patch Richness (PR).

- In 2013, 2018, and 2023, the landscape indices playing a major explanatory role in urban green space carbon sequestration in the Zhengzhou metropolitan area were CWED (30%), IJI (29%), and SPLIT (55%), respectively.
- Increasing the shape complexity of landscape patches, enhancing the average contact between patches and adjacent patches of other types, and reducing the size of urban blocks can increase the carbon sequestration potential of urban green spaces.

1. Introduction

In this chapter, I will introduce the research background and relevant keywords in this thesis. I conducted a detailed analysis of past research and identified significant research aspects. Finally, the research proposal and workflow will be presented.

1.1. Research background

The research background introduces the disruption of the terrestrial carbon cycle, highlights the importance of urban green space, and discusses how the Chinese government has addressed this situation.

1.1.1. Disruption of terrestrial carbon cycle

The carbon cycle refers to the flow and exchange of carbon elements among various environments on Earth. The terrestrial carbon cycle is a crucial part of global biogeochemical cycling and is deeply intertwined with human well-being and sustainable development (Li et al., 2021), exhibiting a strong correlation with human survival and welfare, such as ecosystem services, food security, and timber production (Beer et al., 2010). In the latter half of the twentieth century, numerous pieces of evidence confirmed human disturbances to the global carbon cycle and its potentially immense impact on the climate system (Friedlingstein, 2015). The connection between carbon dioxide concentrations and climate was established over a century ago. Subsequent evidence has demonstrated the human perturbation of the global carbon cycle and its potentially large implications for the climate system (Yin et al., 2023). **As urbanization intensifies, the balance of the carbon cycle is disrupted.** Ongoing environmental changes are thought to increase global terrestrial carbon absorption. However, increasing evidence suggests that extreme climate events such as droughts or storms could lead to a decrease in regional ecosystem carbon stocks, potentially offsetting the anticipated increase in terrestrial carbon absorption (Reichstein et al., 2013). The complexity is further exacerbated by the emissions caused by vegetation carbon dioxide absorption and changes in land use and land cover (Arneth et al., 2017), such as deforestation (Van Der Irf et al., 2009). **To avoid**

potentially catastrophic impacts, the rapid reduction of anthropogenic CO₂ release is necessary (Keller et al., 2018).

A carbon reservoir refers to natural or artificial storage systems capable of absorbing and storing carbon dioxide or other carbon compounds from the atmosphere. Over the past 50 years, ecosystems have offset 25-30% of CO₂ emissions caused by human activities through carbon sequestration in vegetation and soil (Reichstein et al., 2013). Numerous domestic and international studies have confirmed the positive role of vegetation in offsetting carbon emissions. For example, in the 1980s, the carbon capture capability of terrestrial ecosystems in the northern United States could offset 30%-50% of carbon emissions caused by industrial production (Pacala et al., 2001); terrestrial ecosystems in Europe could mitigate 7%-12% of carbon emissions caused by local industrial production (Janssens et al., 2003). Similar research results exist in China. Enhanced vegetation growth has slowed the human-induced increase in atmospheric CO₂ levels, providing negative feedback on the relationship between climate and the carbon cycle. Urban areas cover 2% of the global land but are responsible for 75% of global carbon emissions (Zhang et al., 2014). Urbanization is profoundly reshaping our planet. Throughout the 20th century, the urban population surged from 220 million to 2.8 billion people. Currently, around 56% of the global population resides in urban areas, a figure projected to reach 68% by 2050 (He et al., 2021; Williams et al., 2015).

1.1.2. Significant carbon sequestration in urban green spaces

In a study encompassing 35 major Chinese cities, the collective carbon storage within the vegetation of urban green infrastructure was estimated at 18.7 million tons, averaging 21.34 tons per hectare. Specifically, in 2010, the total carbon sequestration amounted to 1.90 million tons, with an average annual carbon sequestration rate of 2.16 tons per hectare. (W. Y. Chen, 2015). Furthermore, the role of urban green spaces in mitigating carbon emissions extends beyond the direct emission reductions resulting from increased vegetation biomass. Research indicates that urban green spaces can indirectly reduce carbon emissions by alleviating the

urban heat island effect, thereby reducing energy consumption in urban built-up areas, sometimes even more effectively than vegetation growth carbon sequestration.

On average, a single urban park covering approximately 26.9 ± 1.5 hectares in the Yangtze River Economic Belt region has the potential to mitigate approximately 23.7 ± 1.6 tons of CO₂ emissions (equivalent to 1.08 ± 0.03 tons of CO₂ per hectare) on each summer day, primarily through heat mitigation efforts. Collectively, the 1510 urban parks in the region have the capacity to offset approximately 5.37% of the daily fossil fuel emissions in the Yangtze River Economic Belt area (M. Chen et al., 2023); research in Shanghai's Huangpu District indicates that the carbon emission reduction intensity due to the mitigation of heat effects by urban green spaces can reach up to 55.12 t/ Km², significantly higher than the maximum carbon sink value of 19.54 t/ Km². The phenomenon of urbanization makes the carbon cycle processes in urban areas more complex and severe. Urban green spaces, as the main carbon sink areas within cities, have a carbon sequestration capacity that is significantly stronger than that of non-urban areas, demonstrating a great potential for carbon sequestration. **Therefore, conducting research on urban carbon reservoirs is of great significance.**

1.1.3. Difficulties faced by China

Since 2006, China has overtaken the United States to claim the title of the world's largest emitter of carbon dioxide (Maheen et al., 2023), accounting for about 30% of global emissions, and it is expected to reach its peak emissions between 2023 and 2030. From 1980 to 2006, China's carbon emissions from the combustion of fossil fuels increased nearly fourfold. According to China's apparent carbon emission inventory, the country's total surface carbon emissions grew from 3,026.04 million tons in 1997 to 10,434.85 million tons in 2019, an increase of 344.84% over 22 years (Y. Guan et al., 2021; Shan et al., 2018, pp. 2016–2017, 2020, pp. 2016–2017).

With growing public and governmental concern over international environmental issues, China has faced significant pressure in international negotiations on controlling carbon dioxide

emissions and mitigating climate change. In response, the Chinese government has set a series of emission reduction targets and approved the Paris Climate Agreement in 2016, committing to reduce its carbon intensity by 60% to 65% from the 2005 levels by 2030 (Cai et al., 2018; Jacquet & Jamieson, 2016). **It has proposed a range of policies, such as optimizing the energy structure and developing renewable energy sources, to achieve these goals.**

1.2. Relative concept

This chapter includes the definition and relative research about “carbon sequestration” and “urban green space”.

1.2.1. Carbon sequestration

Carbon sequestration refers to the process of removing carbon atoms from the atmosphere over a specific period and storing them in media capable of long-term carbon storage, such as oceans, soils, biota, and plants (Lal, 2008). Carbon sequestration can partially offset anthropogenic greenhouse gas emissions, making it an essential component of global efforts to mitigate climate change (Don et al., 2024). Scholars typically define entities that emit carbon into the atmosphere as carbon sources and those that absorb and store carbon in vegetation or soil as carbon sinks. In the field of urban ecology, common subjects of study regarding carbon sinks include soil carbon sinks and plant carbon sinks, effectively storing atmospheric carbon in soil or the trunks of plants. However, it is crucial to note that ecosystems fix carbon from the atmosphere through photosynthesis and store it in organic matter temporarily, not permanently. The goal of carbon sequestration is to achieve a dynamic equilibrium between carbon released into the atmosphere and carbon stored in soil and vegetation.

Globally, approximately 4.1 billion hectares of forest ecosystems are the main reservoirs of terrestrial carbon (Lal, 2005). A study on the carbon sequestration capacity of China's forest systems showed that **between 2004 and 2008, the total amount of carbon sequestered by forests in China reached an average of 0.36 Pg C/ yr (1 Pg = 10¹⁵g), with 0.30 Pg C/ yr stored**

in vegetation and 0.06 Pg C/ yr stored in surface soils less than 1 meter deep. This sequestration capacity can offset 21% of the country's annual carbon emissions (D. Wang et al., 2014). Regarding vegetation carbon sequestration, there are significant differences in the sequestration capacity among different plant species (Lal, 2005).

1.2.2. Urban green space

Urban green spaces serve as key areas for carbon sequestration within cities, playing a unique role and significance in urban areas. These green spaces are strongly associated with various academic fields such as Environmental Sciences, Urban Studies, Ecology, Public Environmental Occupational Health, Geography, and Regional Urban Planning. The term "urban green space" can encompass various types of vegetation in urban areas, including forests, grasslands, wastelands, and wetlands. However, definitions can vary across sub-disciplines and even among researchers within the same field (Q. Zhou et al., 2022). For instance, in the field of landscape architecture, Malaysian researchers like Nor Akmar define "urban green space" to include forests, parks, water bodies, and recreational or sports sites (Nor Akmar et al., 2011); others define "urban green space" as areas covered with greenery, including streets with sparse landscapes, tree-lined walkways, playgrounds, and forest parks (Almanza et al., 2012). Furthermore, According to (Ambrey & Fleming, 2014), "urban green space" refers to areas delineated using Geographic Information Systems (GIS), including parks, community gardens, cemeteries, sports fields, national parks, and wilderness areas. In ecology, "urban green space" is defined as areas that contribute to the ecological, aesthetic, or public health needs of urban environments (Silaydin Aydin & Çukur, 2012). Some also consider "urban green space" to include urban farms and peri-urban woodlands, offering urban residents opportunities for 'serious leisure' activities such as food or wood production (Yokohari & Bolthouse, 2011).

Overall, there are typically two interpretations: the first regards green spaces as regions with water or vegetation in landscapes, including forests, wilderness areas, street trees, parks, gardens, backyards, geological features, farmlands, coastal areas, and food crops. This

interpretation encompasses the broader concept of natural or semi-natural areas (McIntyre et al., 2008). The second interpretation pertains to urban vegetation, encompassing parks, gardens, yards, urban forests, and urban farms, typically linked with variations of open-space vegetation. This interpretation can be seen as a subset of the broader concept of green spaces but restricted to urban settings. It also serves as a subset of open spaces, emphasizing the central focus of the examined papers on urban landscapes and underscoring the significant human influence on (and reliance upon) urban green spaces. (Kumar et al., 2010). Urban green spaces are fundamental for directly enhancing carbon sequestration and indirectly reducing emissions (F. Xu et al., 2023). By the end of 2010, the total area of urban green spaces (a major component of urban greening infrastructure) accounted for 7.657% of the total urban green space area in 51 Chinese cities. Studies show that urban ecosystems store a significant amount of carbon, with global urban ecosystem carbon stocks estimated at 29.3 Pg C (ranging from 9.3 to 49.3 Pg C), equivalent to 5.3% and 1.8% of the global terrestrial ecosystem's vegetation and soil carbon stocks, respectively (Ge & Zhao, 2017, pp. 1978–2014). A study conducted in the United States in 2010 found that human settlements, both in urban (23–42 kg C /m²) and exurban areas (7–16 kg C /m²), have the potential to store comparable amounts of carbon per unit area. These figures are comparable to the carbon density observed in tropical forests, which are renowned for having the highest carbon density among natural ecosystems, ranging from 4–25 kg C /m² (Churkina et al., 2010).

1.3. International research progress

This chapter introduces the current development process in this academic field. And make a summary of past research methods.

1.3.1. Bibliometric analysis in the field of carbon sinks in urban green spaces

Based on the Web of Science Core Collection database and drawing on previous literature bibliometric analysis and statistical methods (C. Chen et al., 2014; C. Chen & Leydesdorff, 2014; C. Chen & Song, 2019; Hou et al., 2018; Sabe et al., 2022), a literature search was conducted

for the period 1900-2023 using the keywords (“green space”) AND (“carbon stock” OR “carbon sequestration” OR “carbon storage”) AND (“urban” OR “city”). **A total of 387 documents were retrieved**, involving 178 publishers, 2037 authors, and 225 research countries or regions (as of October 14, 2023). The statistical results revealed that research in the direction of urban green space carbon storage began in 2006 and has been accelerating ever since. Around 2011, the field saw its first rapid increase in research activity; a second significant surge occurred in 2021. Since the literature statistics do not include the full year of 2023, they cannot represent the total number of publications or citation frequency for 2023 (Figure 1-1). However, with the deepening of urbanization and increasing societal attention to urban microclimates and ecological health issues, there is good reason to believe that this field has significant prospects for development and expansion.

The research is primarily concentrated in regions such as **China** (136 publications), the United States (72 publications), Germany (33 publications), the United Kingdom (29 publications), Australia (21 publications), and Italy (20 publications). The United States was the first to present studies in this field in 2006, followed by the United Kingdom in the subsequent year, with China, Australia, France, and other countries beginning their research in 2009. Currently, the Chinese Academy of Sciences is the largest contributing institution within the search criteria, having published 30 articles related to the field; followed by Humboldt University of Berlin in Germany, which has 15 articles included in the search (Figure 1-2).

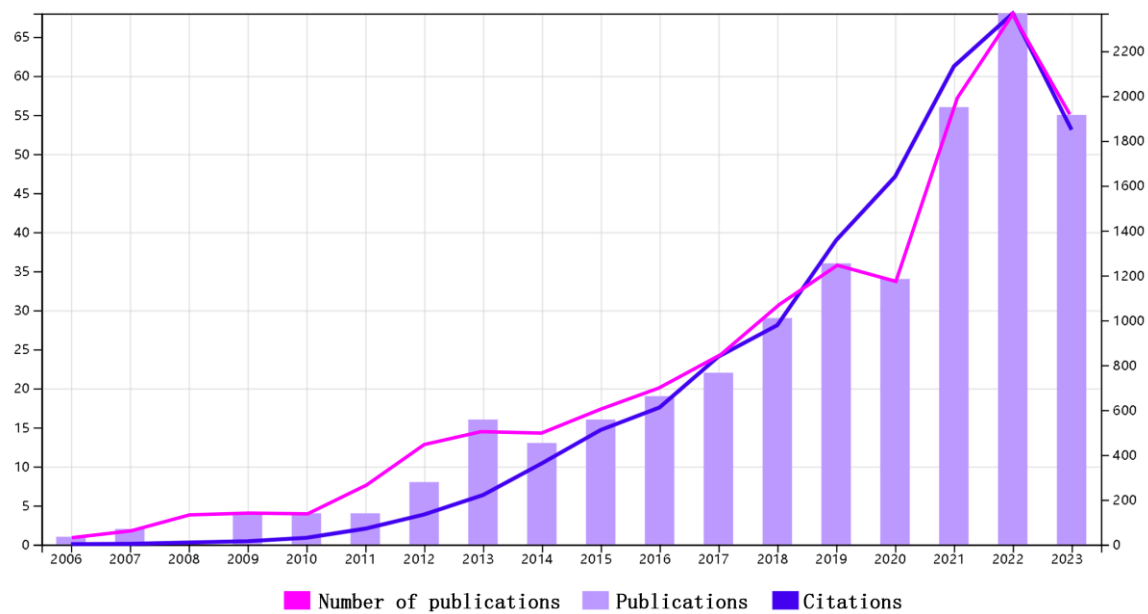


Figure 1-1 Dynamics of the number of documents based on the Web of Science core ensemble

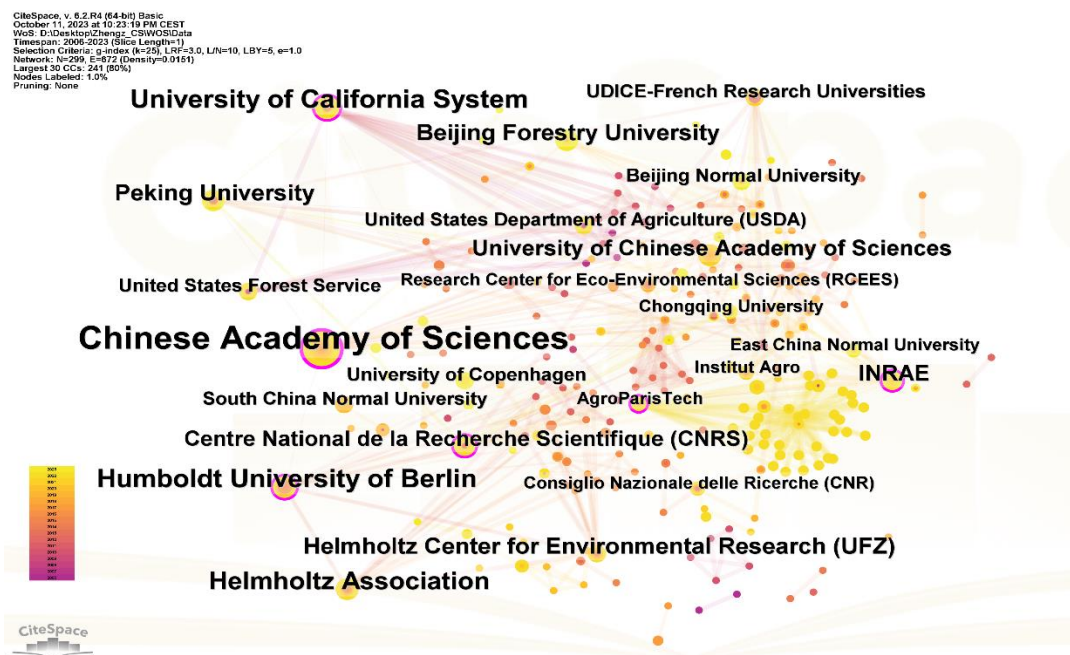


Figure 1-2 Literature research organizations based on the Web of Science core collection

Keywords in scientific literature are terms selected and created by authors, often considered core elements summarizing and representing the content of scientific publications (Lu et al., 2020). In this study, an analysis of keywords from the retrieved 387 articles was conducted (see Figure 1-3), where the size of the circular nodes in the keyword map positively correlates

with the frequency of corresponding keywords. After merging semantically similar terms, high-frequency keywords include: **“carbon storage”, “ecosystem service”, “green space”, “urbanization”, “biodiversity”, “city”, “vegetation”, and “land use”**, among others. Additionally, to further understand the research directions and frontiers in this field during different periods, the Citespace mutation detection algorithm was used to extract burst keywords from the selected literature (see Figure 1-4). Burst keywords refer to terms that experience a sudden increase in occurrence, mentions, or citation frequency within a certain period, often representing the research focus of scholars in the field during that time frame. From Figure 1-4, it can be observed that in the last decade, research directions in the field of urban green space carbon storage have gradually shifted towards mitigating carbon neutrality and reducing carbon emissions.

The Paris Agreement was signed in the United States on April 22, 2016, and took effect on November 4 of the same year. This agreement, proposed during the conference held in France by representatives of 200 countries, aims to achieve net-zero emissions by the latter half of this century. By 2022, over 130 countries and regions have proposed "zero carbon" or "carbon neutrality" climate targets (Y. Zhao et al., 2022). The role of urban green spaces in addressing carbon emissions extends beyond carbon sequestration resulting from vegetation biomass growth. Mitigating the urban heat island effect through urban green spaces and enhancing ecosystem services are gradually becoming the forefront of the industry.

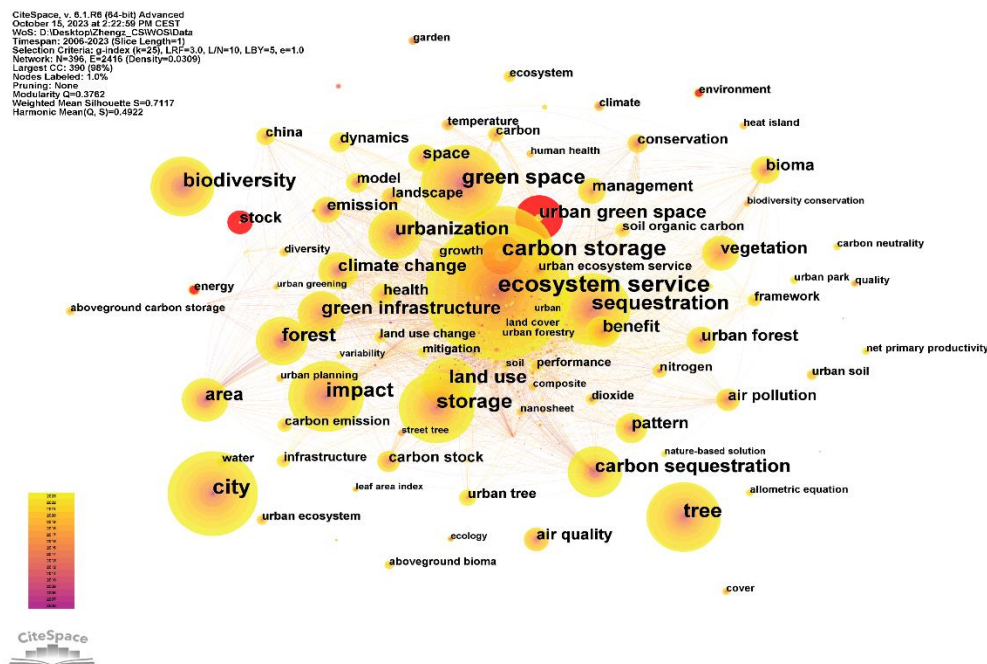


Figure 1-3 Literature keywords based on Web of Science core ensemble

Top 9 Keywords with the Strongest Citation Bursts

| Keywords | Year | Strength | Begin | End | 2006 - 2023 |
|----------------------------|------|----------|-------|------|-------------|
| energy | 2013 | 3.2 | 2013 | 2015 | |
| urban green infrastructure | 2015 | 3.06 | 2015 | 2016 | |
| carbon stock | 2016 | 3.54 | 2018 | 2020 | |
| human health | 2017 | 3.61 | 2019 | 2021 | |
| stock | 2018 | 3.63 | 2020 | 2023 | |
| urban space | 2020 | 2.95 | 2020 | 2023 | |
| carbon neutrality | 2021 | 3.99 | 2022 | 2023 | |
| carbon emission | 2011 | 3.04 | 2022 | 2023 | |
| biomas | 2020 | 2.98 | 2022 | 2023 | |

Figure 1-4 View of mutated keywords in the literature based on the Web of Science core ensemble as well as time zones

1.3.2. Methodology for estimating carbon sequestration in urban green spaces

The concept of carbon sequestration in green spaces originated from research initially focused on estimating forest biomass. By measuring forest biomass and applying specific conversion ratios, researchers began estimating carbon storage in forests. This research gained momentum in the mid to late 20th century, with global studies emerging on carbon storage

estimation. For instance, in the 1950s, researchers conducted plot surveys to gather foundational data, analyzing carbon source and sequestration distributions. They highlighted human activities and deforestation as factors reducing the global forest ecosystem's carbon sink capacity.

Since then, research on forest carbon sequestration has flourished, yielding various estimation methods and findings. Estimation methods for urban green space carbon sinks have evolved from those used in forest studies. However, urban green spaces exhibit unique characteristics compared to forests, including complex spatial distributions, higher species diversity, and increased human impact. Consequently, replication of forest carbon sequestration estimation methods for urban green spaces is not entirely feasible.

This chapter, based on existing literature, organizes the monitoring methods for urban green space carbon sequestration and elaborates on the estimation methods for carbon sequestration in urban green spaces. Urban green spaces play a critical role in urban ecosystems, acting as important carbon sinks that help mitigate the effects of climate change by absorbing CO₂ from the atmosphere. The estimation of carbon sequestration in urban green spaces involves various methods, including **direct measurement of biomass, use of remote sensing technology, and application of mathematical models** to estimate the carbon storage and sequestration potential.

Methods often consider factors such as the type of vegetation, age, density, and the specific urban context to accurately estimate the carbon sequestration capacity. These methods also consider the dynamic nature of urban green spaces, including changes due to urban development, management practices, and natural growth or decline of vegetation. The integration of these methods provides a comprehensive understanding of the carbon sequestration potential of urban green spaces, contributing to urban planning and management strategies aimed at enhancing urban sustainability and resilience to climate

change.

a) Sample plot inventory methods

The plot survey method involves establishing typical plots for field research within the study area to collect relevant data and continuously observe carbon storage information. It estimates carbon storage by applying carbon content conversion coefficients, including the biomass conversion factor method, average biomass method, and model estimation method.

This method calculates biomass by relating stock volume to biomass, using resource inventory data to determine the total stock volume of forest stands from statistical data. Widely used at regional and national scales, it requires adjustments for local conditions and tree species to enhance accuracy.

Using tree data from plots, this method constructs tree models or simulates tree growth, inputs vegetation information from remote sensing images, and estimates the study area's carbon sink capacity. Models like i-Tree, Citygreen, ThePathfinder, InVEST, and the National Tree Benefit Calculator offer various approaches. While i-Tree is suitable for large-scale urban green spaces like urban forests and parks, Citygreen estimates carbon sequestration of individual street trees and urban forests. The Pathfinder calculates comprehensive carbon data and InVEST focuses on land use information and carbon storage relationships at urban regional scales. The National Tree Benefit Calculator estimates the carbon sequestration of individual plants. Compared to traditional methods, these models save labor and resources, enabling quicker, more efficient, and comprehensive estimations. However, since most models were developed abroad, researchers often adjust parameters using U.S. cities with similar climates to reduce computational errors.

b) Assimilation and micrometeorological methods

The assimilation method estimates plant net carbon sequestration by measuring

photosynthetic physiological indicators, such as stomatal conductance and net photosynthesis rate, along with structural parameters like green mass and leaf area. Scholars have applied this method to study urban green space species, aiding in the selection of high carbon sequestration tree species for different regions. The micrometeorological method measures gas flux values by assessing turbulence conditions and gas concentration in the near-ground layer, allowing direct, continuous detection of CO₂ flux between green spaces and the atmosphere. The eddy covariance technique, a representative method, facilitates this measurement. Saleh Shadman et al. used eddy covariance technology to measure CO₂ flux in Helsinki's Hyväntoivonpuisto Park, guiding carbon sink enhancement design in the Jätkäsaari demonstration area within the park. While offering direct, accurate, and continuous monitoring, this method requires stable underlying surfaces. Research indicates significant variations (80%-100%) in carbon sink values measured in atmospherically unstable locations and complex terrains compared to other methods. Moreover, it's limited to point observations, posing challenges for medium and large-scale assessments.

3) Remote sensing estimation methods

Remote sensing technology, known for its real-time, wide-ranging acquisition, and rapid processing capabilities, combined with field survey data and driven models, is an effective method for estimating carbon sinks. Carbon sink estimation using remote sensing technology is mainly divided into two types: inversion estimation and model simulation.

The first one involves obtaining carbon storage data through field surveys and extracting remote sensing parameters like NDVI and EVI from remote sensing imagery. A fitting equation is established between these parameters and the carbon storage data, enabling estimation of carbon storage for the entire area; Second one monitoring urban green space carbon sinks through model simulation involves parameter models and process models. Parameter models, also called semi-empirical models, estimate carbon flux sizes using empirical formulas based on various related parameters, such as the CASA light use efficiency model. Process models

simulate vegetation photosynthesis, transpiration, respiration, and their exchange with the environment based on the physiological and ecological processes of forest ecosystems.

1.4. Research content

- 1) Modelling the relationship between vegetation index and carbon sequestration.
- 2) Estimating the spatial and temporal variation of carbon sequestration in Zhengzhou metropolitan area.
- 3) Performance of landscape indices.
- 4) Correlation between different landscape pattern indices and carbon sequestration.

1.5. Research proposal

Through the development of the aforementioned research content, the following research objectives are achieved:

- Clarify the distribution and spatial and temporal changes of carbon sequestration in urban green spaces within the Zhengzhou metropolitan area.
- Analyze the correlation between carbon sequestration and landscape patterns.
- Explore the influencing landscape indices of carbon sequestration in urban green spaces.
- Provide guidance for the construction and quality improvement of UGs, contributing to the achievement of carbon neutrality.
-

1.6. Technological route

Here is the workflow of the full thesis.

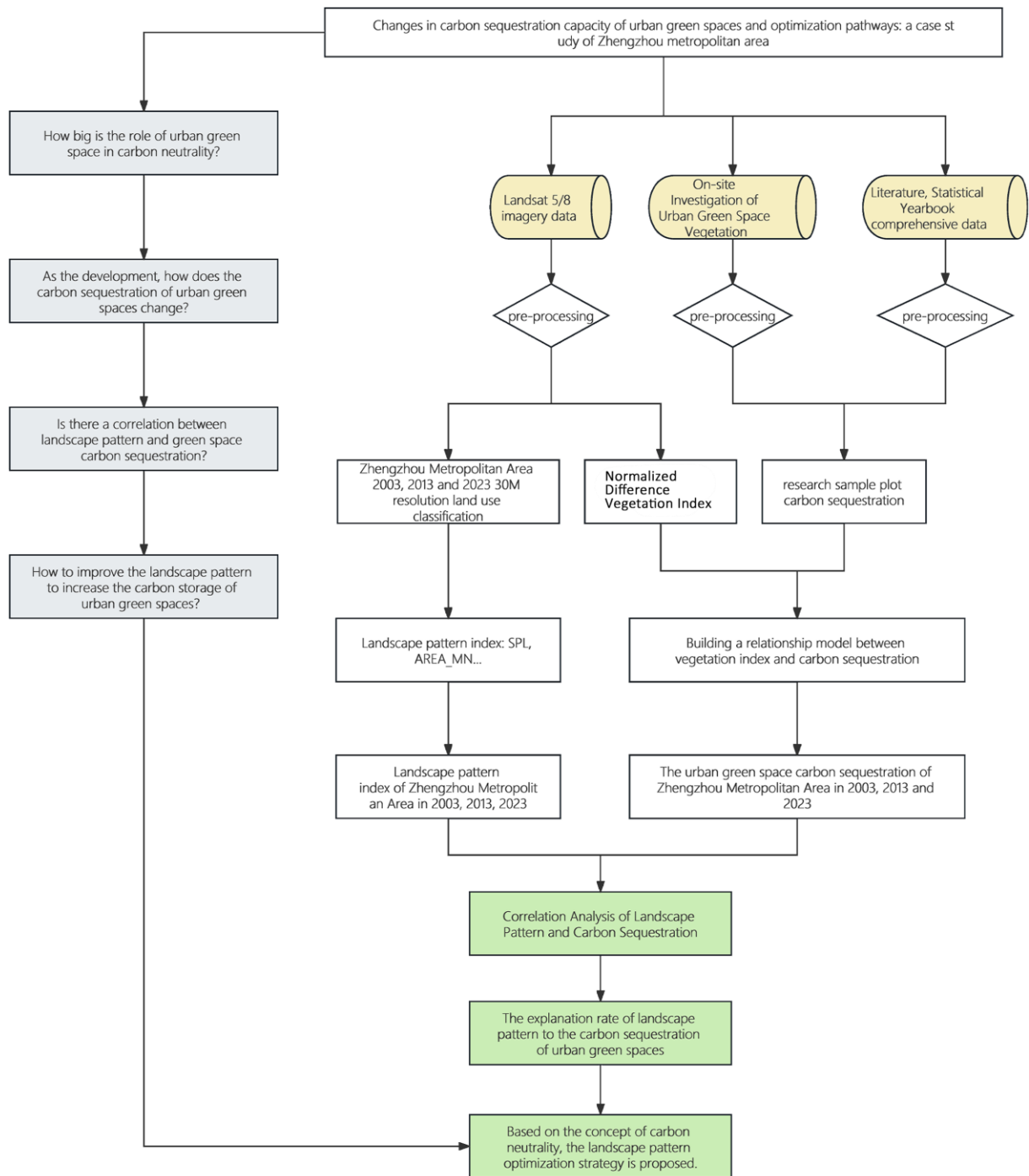


Figure 1-5 Research flow

2. Materials and Methods

This chapter will introduce the research area and research method used in this thesis.

2.1. Research area

The Zhengzhou metropolitan area (Figure 2-1), located in central China in the middle and lower reaches of the Yellow River, consists of nine peripheral cities closely linked in terms of socio-economic activities, including **Zhengzhou, Kaifeng, Luoyang, Pingdingshan, Xinxiang, Jiaozuo, Xuchang, Luohe, and Jiyuan**. As of 2022, the Zhengzhou metropolitan area covers an area of approximately 58,800 square kilometers, with a total economic output of 3.28 trillion yuan and a permanent population of 46.7 million.

Located centrally within China, the Zhengzhou metropolitan area benefits from its strategic position at the convergence of three national transportation corridors: the Heihe-Hong Kong-Macao corridor, the Yantai-Chongqing corridor, and the land bridge. This advantageous geographical position is supported by robust transportation infrastructure. The comprehensive transportation network has reached 103,000 kilometers. The 2023 "Development Plan for the Zhengzhou Metropolitan Area" emphasizes ecological construction and continues to promote a green transformation in production and lifestyle. With the theme of green and low-carbon development, it strengthens the joint governance of the ecological environment and focuses on constructing an organically connected ecological network while promoting energy conservation and carbon reduction. Therefore, the Zhengzhou metropolitan area is an ideal region for studying urban green space carbon sequestration.

This paper selects the main built-up areas of nine cities within the Zhengzhou metropolitan area as the study area, as outlined in section 2.3.1. As the concept of the Zhengzhou metropolitan area is relatively new and there is no specific data available for it, this study focuses on exploring the nine cities included in it separately.

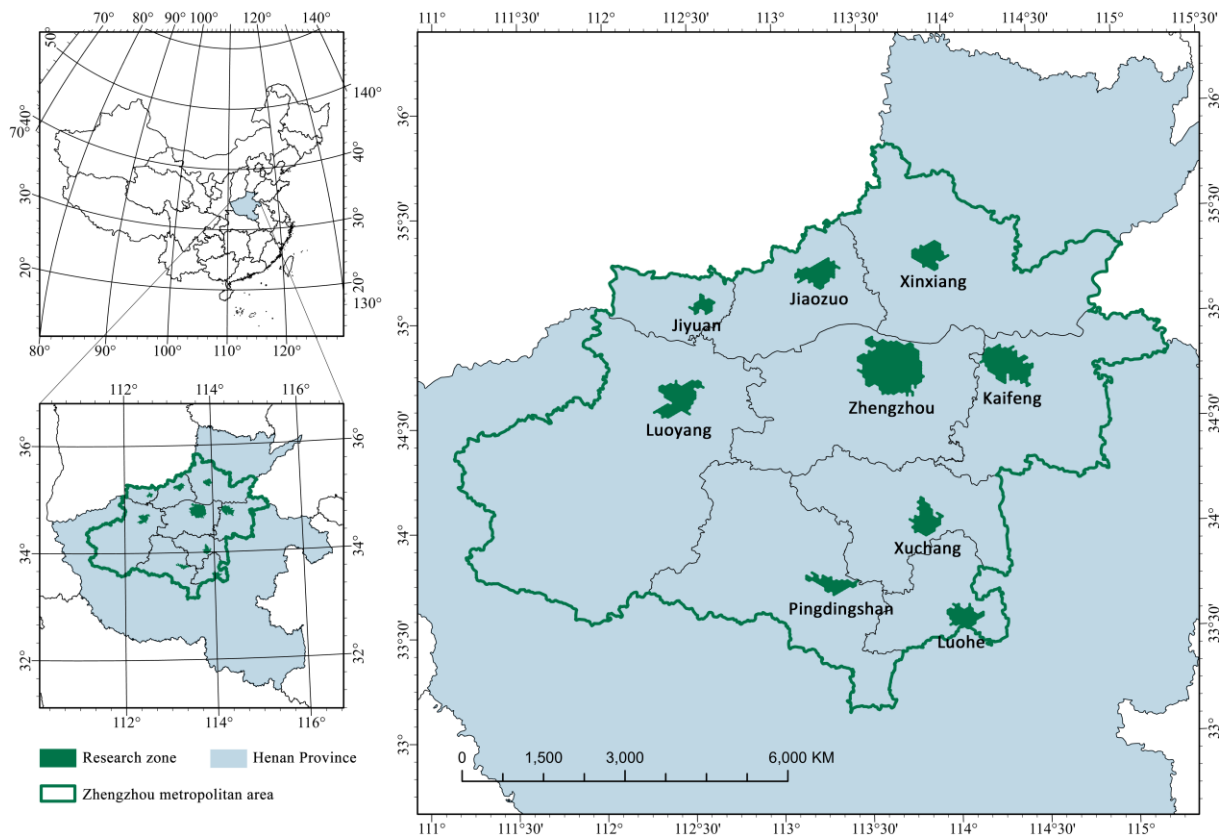


Figure 2-1 Map of the study area

The population density differences among the nine cities in the Zhengzhou metropolitan area are significant (Table 2-1). Zhengzhou has the highest population density (1708 people/square kilometer), ranking second in population, which is 1.89 times higher than that of Luohe (902 people/square kilometer), the city with the lowest population density, and 4.67 times higher than that of Jiyuan (366 people/square kilometer). The variation in city size is also evident, with Luoyang being the largest in the area at 15,492 square kilometers and a total population of 7,079,000, ranking second among the cities in the Zhengzhou metropolitan area, following only Zhengzhou. Despite being third in the area (7,507 square kilometers), Zhengzhou ranks highest in population within the Zhengzhou metropolitan area, reaching 12,828,000 people. Zhengzhou's overall GDP far exceeds that of other cities, reaching 1,827.60 million USD in 2023, with a per capita GDP of 14,295 USD. However, it is noteworthy that despite Jiyuan having a smaller population, its per capita GDP surpasses that of Zhengzhou, reaching 15,615 USD, despite its overall GDP being at the bottom of the nine cities at 113.91

million USD in 2023.

The climate of the Zhengzhou metropolitan area predominantly falls within the warm temperate zone, transitioning to the subtropics in its southern region. It features a continental monsoon climate with relatively consistent temperatures across its cities. In 2023, the average annual highest temperature at around 22 degrees Celsius, while the average annual lowest temperature was approximately 10 degrees Celsius. However, there are significant differences in rainfall. Xuchang, located in the warm temperate monsoon region, experiences distinct four seasons with an annual rainfall of 3370.7mm, significantly higher than other cities. Additionally, Jiaozuo also has rainfall exceeding 1000mm (1243.2mm), while Pingdingshan had the highest number of rainy days in 2023, reaching 81 days. Conversely, Xinxiang (497.7mm) and Kaifeng (691mm) have relatively lower rainfall, with both cities experiencing 63 rainy days in 2023.

Table 2-1 General background of 9 cities in Zhengzheng Metropolitan Area in 2023

| City | Area (km ²) | Resident population | Population density (person/ km ²) | GDP (100 million USD) | Per Capita GDP (USD) | Average high temperature (°C) | Average low temperature (°C) | Precipitation (mm/ year) | Precipitation per days (per year) |
|--------------|----------------------------|------------------------|-----------------------------------------------------|-----------------------------|-------------------------|----------------------------------------|------------------------------------|--------------------------------|--------------------------------------------|
| Zhengzhou | 7,507 | 12,828,000 | 1708 | 1,827.60 | 14,295 | 22 | 11 | 958.9 | 63 |
| Kaifeng | 6,247 | 4,694,000 | 751 | 375.44 | 7,923 | 22 | 11 | 691 | 63 |
| Luoyang | 15,492 | 7,079,000 | 456 | 801.87 | 11,336 | 21 | 10 | 840.9 | 68 |
| Pingdingshan | 7,874 | 4,961,000 | 630 | 401.18 | 8,081 | 20 | 9 | 713.7 | 84 |
| Xinxiang | 8,629 | 6,166,000 | 714 | 489.44 | 7,935 | 22 | 10 | 497.7 | 63 |
| Jiaozuo | 4,072 | 3,523,500 | 864 | 315.76 | 8,963 | 22 | 11 | 1243.2 | 73 |
| Xuchang | 4,977 | 4,381,000 | 880 | 266.98 | 12,083 | 22 | 10 | 3370.7 | 66 |
| Luohe | 2,617 | 2,368,000 | 902 | 256.15 | 10,808 | 22 | 11 | 917.9 | 73 |
| Jiyuan | 1,965 | 729,000 | 366 | 113.91 | 15,615 | 22 | 10 | 775.7 | 72 |

2.2. Extract the main built area of cities

The scope of this study focuses on urban green spaces, and before the formal research begins, it is necessary to first determine the extent of the urban built-up area. The built-up area is defined by extracting the administrative boundaries of the main urban areas of each city. Initially, the land use classification data for the year 2023 is calculated using specific classification methods as described in section 2.4.1. Due to the impact of urbanization and urban expansion, the built-up area in 2023 is larger than in all previous years (M. Xu et al., 2016).

Firstly, based on the results of the land use classification data, a hexagonal grid of 960 meters in length is established for the Zhengzhou metropolitan area (see Figure 2-2). Subsequently, **grid cells with built-up areas exceeding 50% are selected, and those cells are defined as built-up areas**, while the rest are excluded (Y. Zhou et al., 2018). Since some main urban areas contain large areas of development land, large parks, or water bodies, a manual visual identification method is applied to further refine the main urban area boundaries and the grid cells within these boundaries.

Next, the outer contour of the hexagonal grid is extracted to serve as the original boundary of the urban built-up area. **A smoothing line method is then applied to further process the original boundary of the urban built-up area**, resulting in the final delineation of the main urban area boundaries for this study.

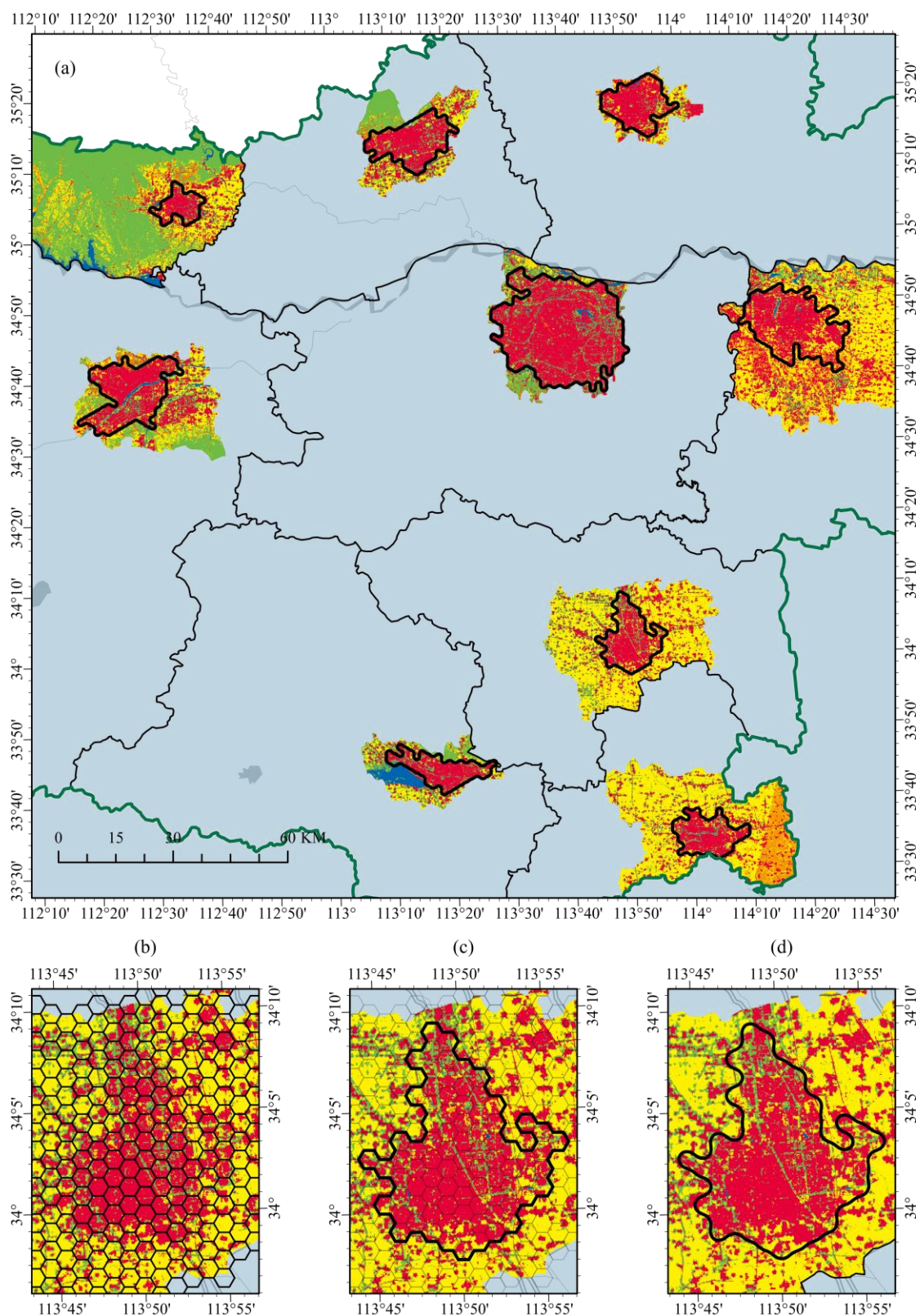


Figure 2-2 Built area boundaries extract

(a) Built area boundaries of 9 cities (b) Create hexagon for Xuchang as an example (c) Extract built area boundary of Xuchang as an example (d) Smooth the boundary of Xuchang as an example

2.3. Sample point setting and field survey

This chapter will introduce the process of selecting plots for field research and detail the methodology employed in conducting the field research.

2.3.1. Set plots for field research

This study is based on biomass and plant allometric equations to estimate the carbon sequestration capacity within the sample plots, thus necessitating a survey of the physical characteristics of plants within these plots. The survey was conducted from **June to August 2022** to ensure that the plants were at their maximum biomass period. In determining the built-up areas of 9 cities within the Zhengzhou metropolitan circle, **coordinates were randomly generated using the random sampling method** in ArcGIS Pro, with the stipulation that the adjacent distance between two coordinates should not be less than 100 meters. The number of coordinate points depends on the size of the urban built-up area, with **an average of 1-2 points taken every 4 square kilometers**. With the aid of the latest high-definition remote sensing images from Google Earth Pro 2023, manual visual identification of the coordinate points was carried out, ensuring that each city's built-up area includes five types of green spaces: ancillary green space, regional green space, protective green space, parks, and squares. The vegetation conditions should represent the surrounding vegetation cover and not be accidental. Due to practical limitations, some coordinates located in private areas and those difficult for sampling were omitted. **A total of 974 coordinate points were selected**, as illustrated in Figure 2-3 below:

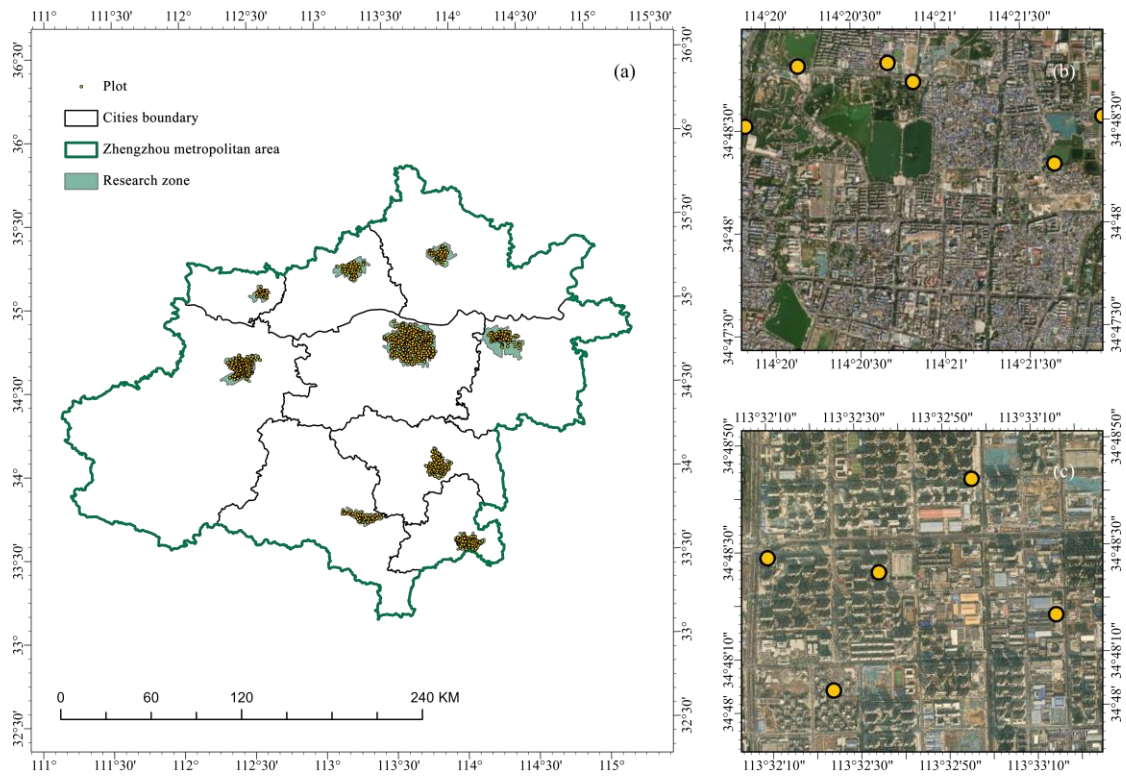


Figure 2-3 Map of plot distribution

(a) Total of plots distribution; (b) Part plots distributed in Xinxiang city as an example; (c) Part plots distributed in Zhengzhou city as an example

2.3.2. Field research

With the 974 coordinate points as centers, circular areas with a diameter of 20 meters are taken to form sample plots with an area of 100π . The vegetation within the sample plots is divided into arboreal, shrub, and ground cover layers, with physical characteristics data of the plants collected separately for each layer. The survey form is shown in Appendix 1. The research team consists of five members (Feng Yuan, Ren Qitan, Yang zhilan, Zhang Mengting, and Lu Xiran), divided into two groups to conduct the surveys, all of whom have backgrounds in forestry or landscape architecture. Before the start of the survey work, field survey standards were established, and all teams underwent field assessments at the same location with uniform training, ensuring each team had uniform high-level field survey capabilities and plant identification skills. Training content includes methodology, sample plot selection, individual tree measurement, green space inspection, photographic recording, and field data entry, among others (Schomaker et al., 2007). The research was completed in June-September

2022 and was supported by the following three research funds: Key Technology R&D Program of Henan Province (232102320190), Special Fund for Young Talents in Henan Agricultural University (30500930 and 30501053) (Figure 2-4).



Figure 2-4 Field research

In this study, trees are classified as species within the sample plot exhibiting a diameter at breast height (DBH), measured as the diameter of the trunk at 1.3 meters above the ground, exceeding 5 centimeters. Shrubs, on the other hand, are identified as tree species lacking a distinct main trunk and typically growing in a clustered configuration (Figure 2-5). All sample plots use the individual tree survey method, with specific survey content as follows:

Basic information: Record the site coordinates and boundary of the plot, the land use type of the site, the proportion of impervious to pervious paving areas, the ground cover plant coverage area, and take photographs for records.

Trees: species, tree DBH, tree height (H), tree crown spread (C), tree branch height, tree east-

west crown spread, tree north-south crown spread, tree crown vacancy rate, tree crown mortality rate, under-crown impervious rate, under-crown shrub rate, and tree sunlight reception. Since the definition of plant health status is somewhat subjective, I decided to use the light transmission rate of the plant canopy as the criterion for evaluating health status. When the plant canopy is almost completely opaque, it is in 100% health condition.

Shrubs: species, shrub vacancy rate, shrub height, shrub basal diameter, shrub crown spread, shrub crown area, and shrub crown volume.

Ground cover: area

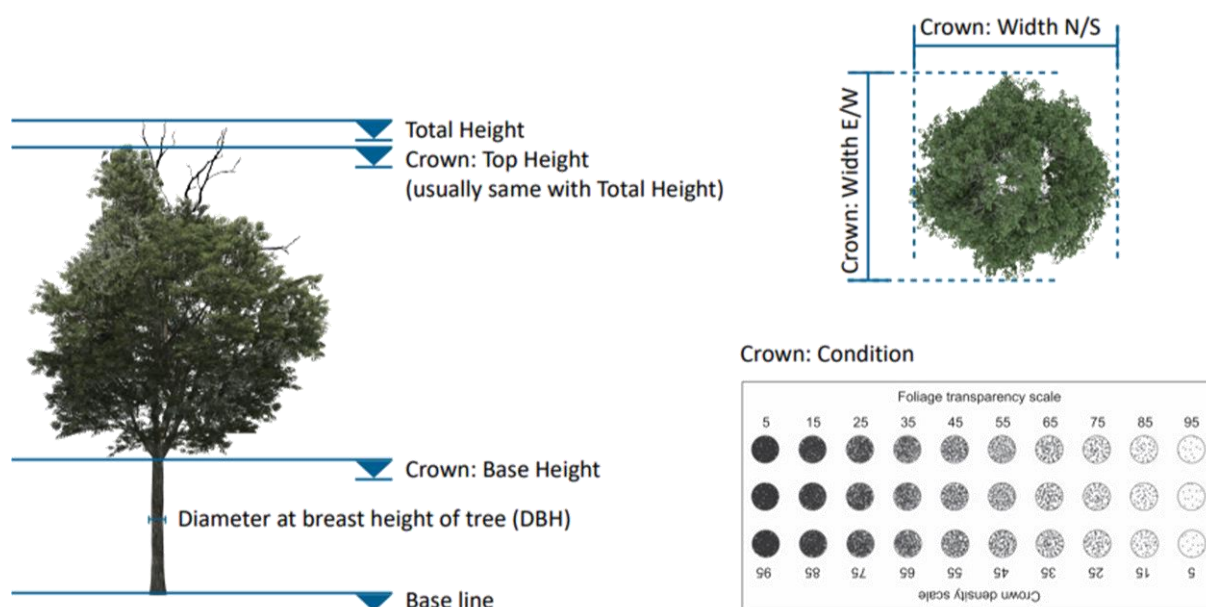


Figure 2-5 Vegetation measurement

After completing all sample plot surveys, the data records of each plot are summarized and entered into a computer for statistical analysis. **In total, 974 sample plots were surveyed, with a total of 25,946 trees investigated.** This includes 349 sample plots in Zhengzhou with a total of 8,744 trees; 148 sample plots in Luoyang with 4,199 trees; 93 sample plots in Kaifeng with 2,890 trees; 74 sample plots in Luohe with 1,229 trees; 30 sample plots in Jiyuan with 1,140 trees; 59 sample plots in Jiaozuo with 1,267 trees; 98 sample plots in Xuchang with 2,610 trees; 65 sample plots in Xinxiang with 2,610 trees; 58 sample plots in Pingdingshan with 1,257 trees.

2.4. Remote sensing image data

The Landsat satellite program, a collaborative effort between NASA and the United States Geological Survey (USGS), aims to monitor Earth's current resources and environmental data. Commencing with Landsat 1's launch in 1972 and continuing through to the latest Landsat 9, this series has consistently provided valuable imagery data with substantial scientific utility over the years. These data cover the globe and possess higher spectral resolution, radiometry, and temporal continuity, thus offering quality and detail that is unmatched by other satellites. The Landsat data have been widely used in numerous scientific fields and various applications, making it one of the most important and extensive means for large-scale surface observation available today (Kovalskyy & Roy, 2013; Zhu, 2019).

This paper utilizes the Level 2 Collection 2 and Tier 1 datasets based on Landsat 8 satellites, with a resolution of 30×30 meters. The Collection 2 dataset is a secondary processing dataset based on the Collection 1 dataset, which significantly improves the absolute geographic coordinate accuracy. Level 2 data originates from Collection 2 Level 1 inputs, conforming to a solar zenith angle of <76 degrees, and incorporates auxiliary data. Tier 1 consists of Level 1 precision and terrain (L1TP) corrected data, ensuring accurate radiometric measurements, and addressing geographic registration challenges when integrating different images. The Landsat 8 satellite has been operational from February 11, 2013, until now, with data calculations for the years 2013, 2018, and 2023 based on Landsat 8 remote sensing imagery.

2.4.1. Land use and land cover data

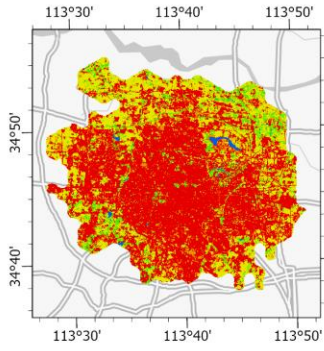
This study employs the Random Forest method to obtain long-term series land use classification data for the study area. Based on cloud cover and the study area, datasets for the years 2013, 2018, and 2023 were selected, with 50, 49, and 57 images respectively meeting the criteria (Appendix 2). Subsequently, masks were applied to remove clouds and shadows and to extract spectral features, and texture features from grayscale images converted from RGB images, and DEM (Digital Elevation Model) features. These features were then merged into a single image for classification. Training samples were created for five categories: water,

green space, built, barren, and crop (Table 2-2), and the classification model was trained on the training dataset and evaluated on the test dataset. The land use classification accuracy was assessed using confusion matrices and Kappa coefficients. The overall accuracy and Kappa index of the land use images for all three years are higher than 0.98, indicating high accuracy. The classification results are shown in Figure 2-6 :

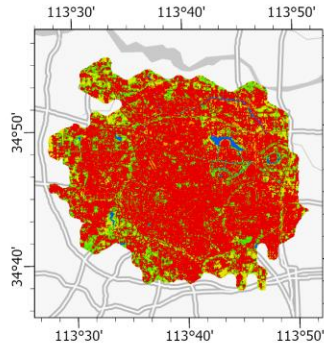
Table 2-2 Description of different classes of land use

| Classification | Description |
|----------------|---------------------------------------------------------------------------------------------|
| Water | Rivers (canals), lakes (banks), ponds, fountains, pools, etc. |
| Green space | Trees, shrubs, natural and artificial grasslands, forests and wetlands |
| Crops | Farmland with regular crop rotation and harvesting, such as paddy fields, and no tree cover |
| Barren | Unutilized land types covered by sand, stone, gravel, etc. |
| Built | Impervious surfaces for buildings, roads, squares, car parks, etc. |

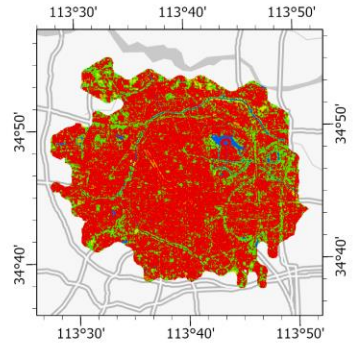
* It is divided by the current utilization of the research zone and the needs of the research



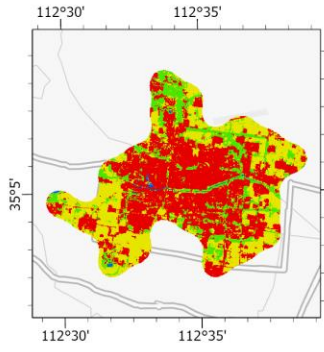
(a1) Zhengzhou 2013 LULC



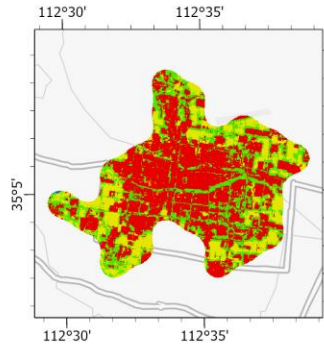
(a2) Zhengzhou 2018 LULC



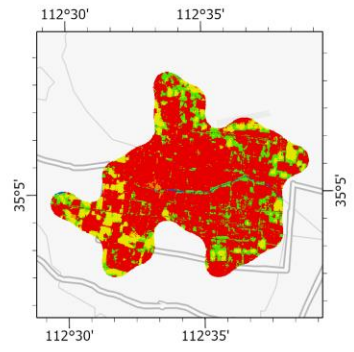
(a3) Zhengzhou 2023 LULC



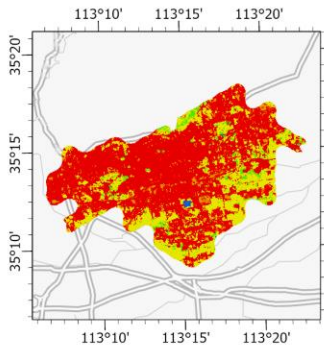
(b1) Jiyuan 2013 LULC



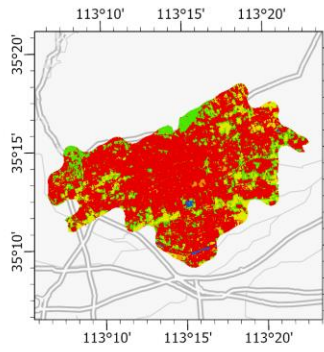
(b2) Jiyuan 2018 LULC



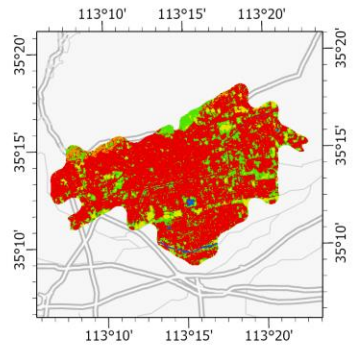
(b3) Jiyuan 2023 LULC



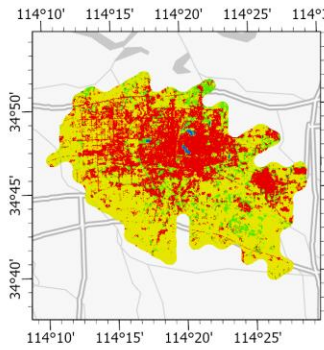
(c1) Jiaozuo 2013 LULC



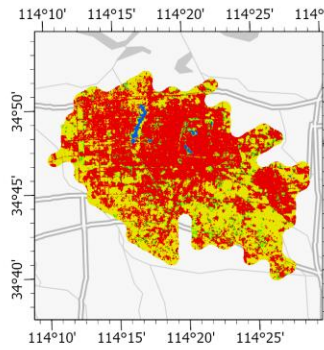
(c2) Jiaozuo 2018 LULC



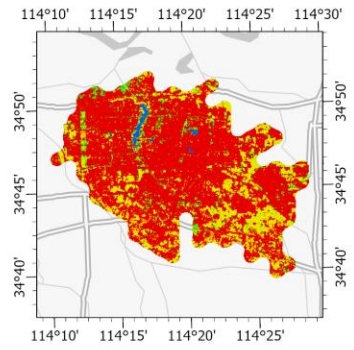
(c3) Jiaozuo 2023 LULC



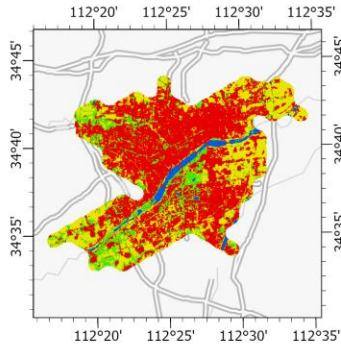
(d1) Kaifeng 2013 LULC



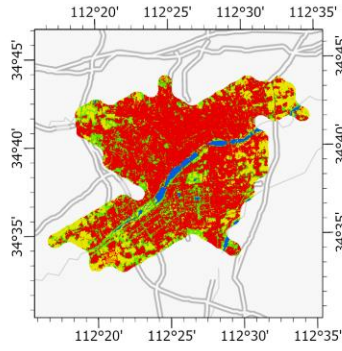
(d2) Kaifeng 2018 LULC



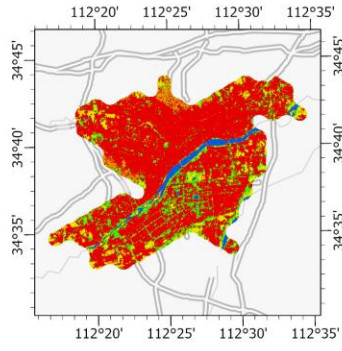
(d3) Kaifeng 2023 LULC



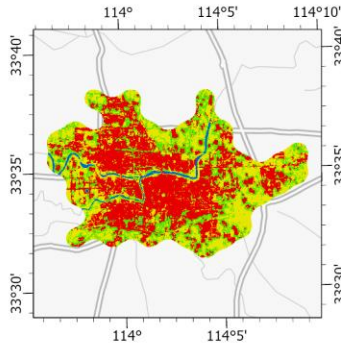
(e1) Luoyang 2013 LULC



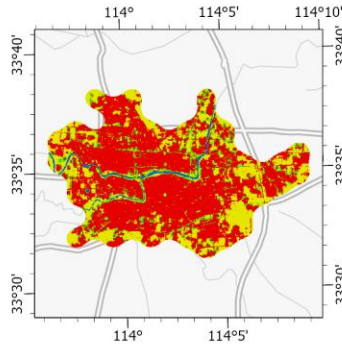
(e2) Luoyang 2018 LULC



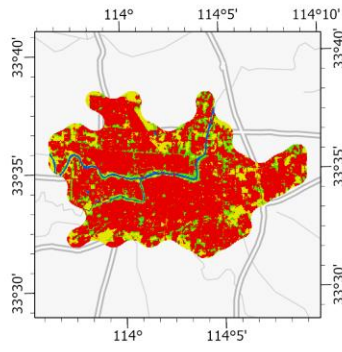
(e3) Luoyang 2023 LULC



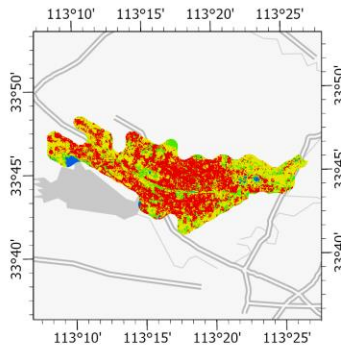
(f1) Luohe 2013 LULC



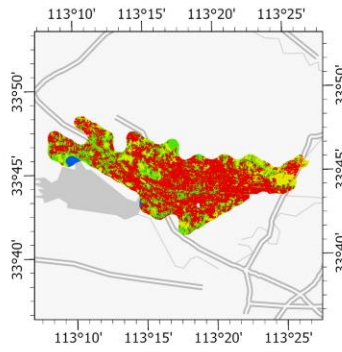
(f2) Luohe 2018 LULC



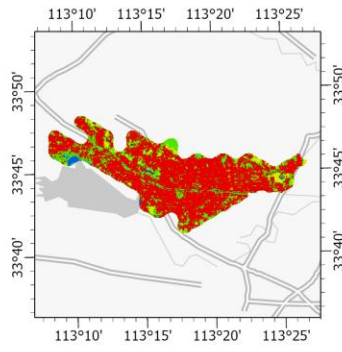
(f3) Luohe 2023 LULC



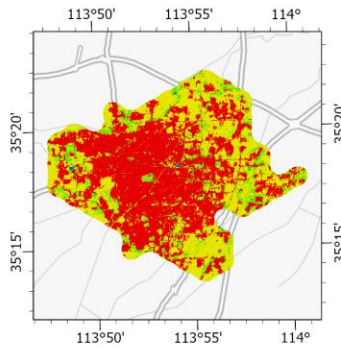
(g1) Pingdingshan 2013 LULC



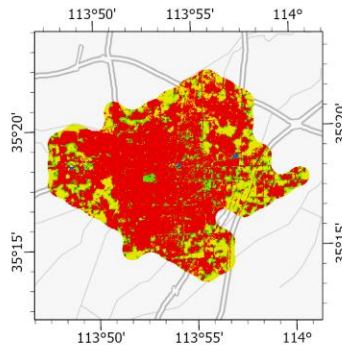
(g2) Pingdingshan 2018 LULC



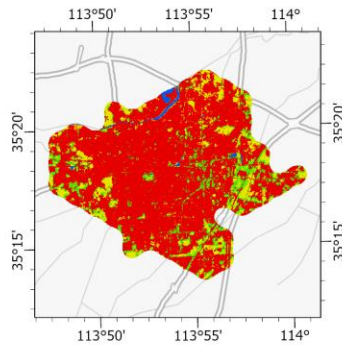
(g3) Pingdingshan 2023 LULC



(h1) Xinxiang 2013 LULC



(h2) Xinxiang 2018 LULC



(h3) Xinxiang 2023 LULC

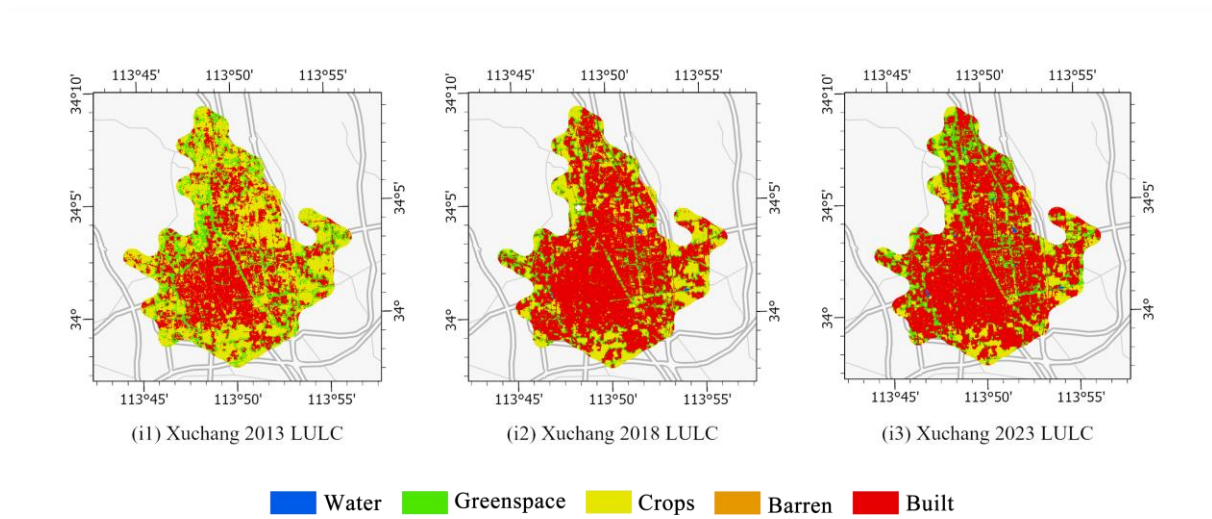


Figure 2-6 Land use and land cover classification

2.4.2. Normalized Difference Vegetation Index (NDVI)

NDVI is computed by subtracting the red-light reflectance from the near-infrared (NIR) reflectance and then dividing the result by the sum of NIR and red-light reflectance. It is one of the key parameters for indicating crop growth vigor and nutritional status:

$$NDVI = (NIR - R)/(NIR + R)$$

Where, *NIR* represents the reflectance in the near-infrared region, which is sensitive to the amount of plant biomass, *Red* represents the reflectance in the red-light region, which is absorbed by chlorophyll for photosynthesis. Negative NDVI values typically indicate water bodies. Water absorbs much of the visible and near-infrared light, resulting in negative values. NDVI values close to +1 suggest dense green leaves. This is because healthy vegetation reflects more near-infrared light and absorbs most of the visible light, especially in the red channel. NDVI values close to 0 often indicate barren areas, rock, or urbanized areas where there's no significant green leaf vegetation. These surfaces do not absorb much visible light or reflect near-infrared light, leading to values near zero. This makes NDVI a useful index for monitoring vegetation health, assessing crop conditions, analyzing land use change, and mapping land cover over large areas using satellite imagery. **In this study, the mean NDVI values for June-September in research zones 2013, 2018 2022, and 2023 were calculated using Landsat**

remote sensing images through the Google Earth Engine platform.

2.5. Quantification of carbon sequestration

The quantification of the carbon sequestration capacity of urban green spaces in this study is mainly based on the sample plot survey data and biomass allometric equations.

2.5.1. Calculation of carbon sequestration capacity of trees

The i-Tree Eco model (Raum et al., 2019), developed by the United States Forest Service, assesses urban forest structure and ecological impacts using field data and local air pollution and meteorological data. It offers various analyses, including species distribution, leaf area, biomass, and ecological benefits such as air pollutant removal, carbon sequestration, oxygen production, and hydrological effects. Researchers utilize i-Tree Eco to quantify the ecological benefits of urban parks and forests, particularly its ability to assess individual plant benefits. The model calculates carbon sequestration by collecting tree data from sample plots and applying built-in growth equations. These equations, based on species, diameter at breast height (DBH), crown width, and other factors, are selected based on proximity to the species (Falster et al., 2015). Input parameters also include local meteorological data and air quality, with substitutes used for cities lacking meteorological station data.

2.5.2. Calculation of carbon sequestration capacity of shrubs

In this study, the carbon sequestration capacity of shrubs is estimated based on the aboveground biomass estimated by shrub individual biomass models compiled from existing research, and the biomass is multiplied by a carbon conversion coefficient of 0.5 to calculate the carbon storage. Furthermore, based on the known carbon storage of individual shrubs, the carbon sequestration amount of individual shrubs is estimated using the conversion coefficients for carbon storage and carbon sequestration of trees belonging to the same genus or family as those in this study.

To obtain a more accurate model for calculating shrub biomass, before starting the calculations in this section, the biomass allometric equations currently available in the relevant literature

are summarized in Appendix 3. Firstly, the shrubs' carbon stocks were calculated by multiplying their biomass by a carbon conversion factor of 0.5. (Houghton, 2005; Nowak & Crane, 2002). The formula for its calculation is:

$$CS_{shrub} = Biomass_{shrub} \times 0.5$$

In the formula, CS_{shrub} represents the aboveground carbon storage of shrubs, measured in kilograms, and $Biomass_{shrub}$ refers to the aboveground biomass of shrubs, also measured in kg.

The carbon sequestration amount of shrubs is calculated using the tree data in this study. Firstly, the carbon storage and sequestration values of trees calculated based on the i-Tree Eco model are organized, and the ratio of carbon storage to carbon sequestration for each tree species category, i.e., the conversion coefficient, is calculated. Secondly, the carbon storage of shrubs is multiplied by the conversion coefficient of trees within the same family to estimate the carbon sequestration number of shrubs. If some shrub families do not have a corresponding tree carbon conversion coefficient, then the average tree conversion coefficient is applied, as shown in Table 2-3 for the "Other Shrubs" category. The conversion coefficients for carbon storage and carbon sequestration of trees and shrubs calculated in this study are shown in Table 2-3. The formula for calculating the conversion coefficient between tree carbon storage and carbon sequestration is as follows:

$$F_f = TC_f / TCS_f$$

In the formula, F_f represents the conversion coefficient between the carbon storage and the carbon sequestration for trees and shrubs belonging to family f . TC_f is the total carbon storage value of trees within family f , and TCS_f is the total carbon sequestration value of trees within family f . The formula for calculating the carbon sequestration amount of shrubs is as follows:

$$CSS_i = CS_i / F_f$$

In the formula, CSS_i represents the carbon sequestration amount of the i -th species of shrubs within family f , CS_i is the carbon storage of the i -th species of shrubs, and F_f is the conversion coefficient between the carbon storage and carbon sequestration for trees and shrubs belonging to family f .

Table 2-3 Conversion factor between carbon stock and carbon sequestration

| Family | Conversion factor |
|----------------|-------------------|
| Cupressaceae | 9.1 |
| Labiatae | 2.47 |
| Rosaceae | 6.77 |
| Oleaceae | 7.81 |
| Malvaceae | 8.07 |
| Lythraceae | 8.38 |
| Leguminosae | 10.48 |
| Caprifoliaceae | 5.37 |
| Caprifoliaceae | 2.48 |
| Apocynaceae | 13.78 |
| Aquifoliaceae | 13.29 |
| Calycanthaceae | 11.05 |
| Adoxaceae | 46.87 |
| Other species | 8.89 |

2.5.3. Calculation of carbon sequestration capacity of ground cover

For ground cover plants, which are often planted as a mixture of multiple species and are difficult to distinguish by species, the calculation of carbon sequestration capacity refers to the research by Shadman (Shadman et al., 2022). **The carbon sequestration capacity of ground cover plants is primarily influenced by the planting area.**

$$Area = \pi r^2$$

Where $Area$ denotes the planting area of ground cover plants and r denotes the planting radius of a circular lawn. Subsequently, the dry weight of the grass was calculated:

$$TDW_{turf} = Area \times 0.56$$

In the formula, TDW_{turf} represents the total dry weight of the groundcover. The carbon stock is equal carbon sequestration, as most of the ground covers are annual plants.

$$CSG_{turf} = TDW_{turf} \times 0.427$$

In the formula, CSG_{turf} represents the carbon sequestration of the ground cover plant.

Calculation of sample carbon sequestration capacity. The plant carbon sequestration capacity of the sample consists of a combination of trees, shrubs, and ground cover plants, calculated as follows:

$$CS_{plot} = (CST_{plot} + CSS_{plot} + CSG_{plot}) / Area_{plot}$$

Where CS_{plot} denotes the density of carbon sequestration in Kg C/m² yr; CST_{plot} denotes the total amount of carbon sequestration in the tree layer in the sample; CSS_{plot} denotes the total amount of carbon sequestration in the shrub layer in the sample; CSG_{plot} denotes the total amount of carbon sequestration in the vegetation layer in the sample; $Area_{plot}$ denotes the area of the sample, which is taken as the value of 100π here.

2.5.4. Calculation of carbon sequestration capacity of urban green space

Based on the sample plot coordinates, a correlation analysis between the NDVI values of the sample plots in 2022 and their carbon storage was conducted. The Pearson correlation coefficient reached 0.735, indicating a significant correlation (Table 2-4).

Table 2-4 Correlation analysis between carbon sequestration and NDVI

| | | NDVI |
|---------------------|----------------------|--------|
| Pearson Correlation | Carbon sequestration | .735** |
| | Sig. (2-tailed) | 0.000 |
| Kendall's tau_b | Carbon sequestration | .654** |
| | Sig. (2-tailed) | 0.000 |
| Spearman's rho | Carbon sequestration | .815** |
| | Sig. (2-tailed) | 0.000 |

** . Correlation is significant at the 0.01 level (2-tailed).

The sample plots were subjected to curve simulation with their corresponding NDVI values for the year 2022 to construct a relationship model (Figure 2-7, Table 2-5). The results revealed that a power function provided the best fit, with an R^2 value of 0.666. Consequently, a power function was used to estimate the interannual changes in carbon sequestration for the Zhengzhou metropolitan area for the years 2013, 2018, and 2023.

$$\text{Carbon sequestration (kg C/m}^2 \text{ yr)} = 3.05 * NDVI^{1.70}$$

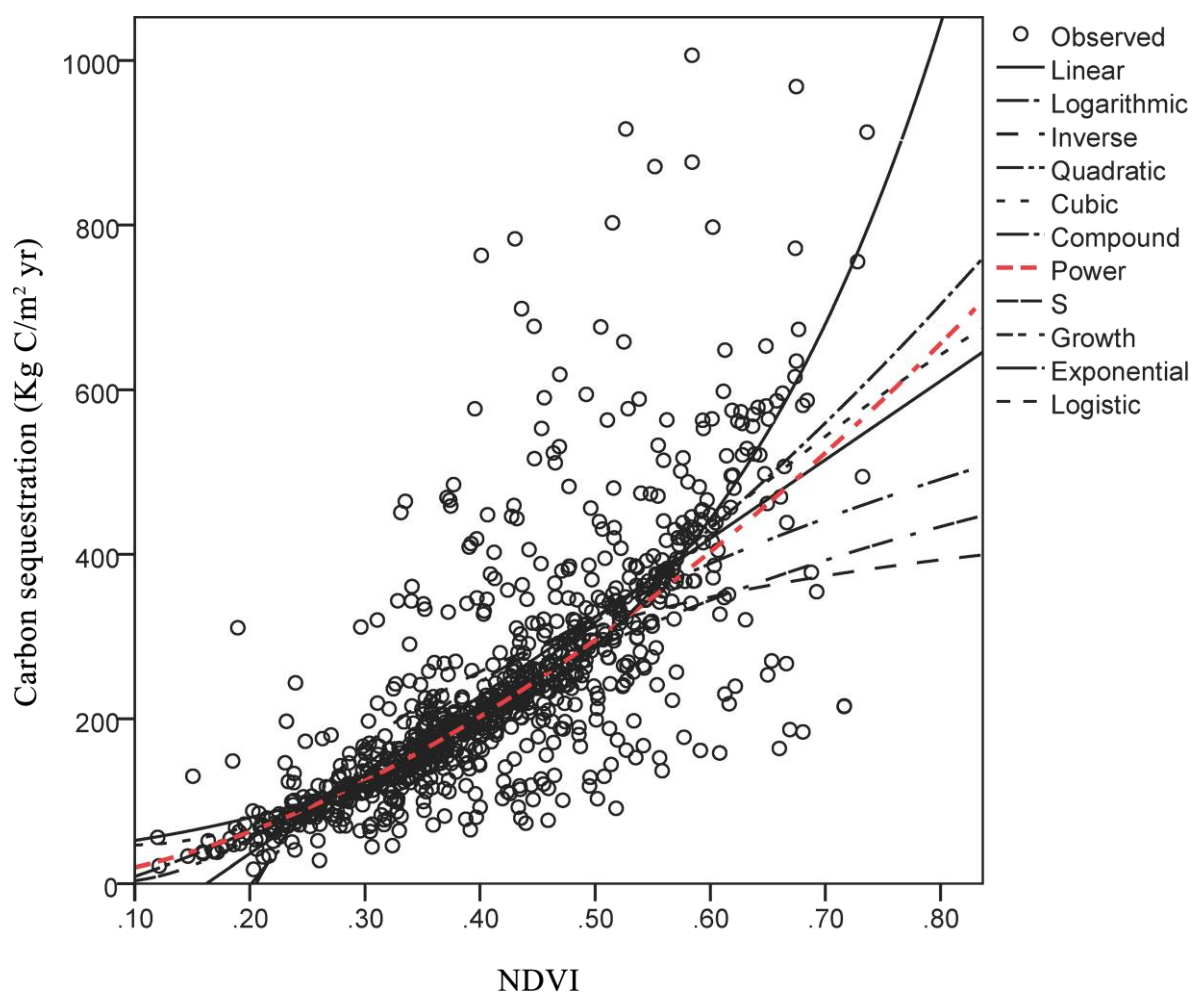


Figure 2-7 Estimation of vegetation carbon sequestration based on the curve of vegetation stock and NDVI value of the same period in the sample

Table 2-5 Estimation of vegetation carbon sequestration based on the curve of vegetation stock and NDVI value of the same period in the sample

| Model Summary | | | | | Parameter Estimates | | | | |
|---------------|----------------|---------|-----|-----|---------------------|----------|---------|---------|----------|
| Equation | R ² | F | df1 | df2 | Sig. | Constant | b1 | b2 | b3 |
| Linear | 0.54 | 1076.39 | 1 | 914 | 0.000 | -155.50 | 957.51 | | |
| Logarithmic | 0.50 | 900.15 | 1 | 914 | 0.000 | 570.55 | 356.16 | | |
| Inverse | 0.41 | 624.01 | 1 | 914 | 0.000 | 529.05 | -108.73 | | |
| Quadratic | 0.55 | 552.55 | 2 | 913 | 0.000 | -31.71 | 328.34 | 737.68 | |
| Cubic | 0.55 | 369.09 | 3 | 912 | 0.000 | 68.99 | -486.93 | 2774.10 | -1586.72 |
| Compound | 0.64 | 1641.32 | 1 | 914 | 0.000 | 33.79 | 72.83 | | |
| Polr | 0.67 | 1820.69 | 1 | 914 | 0.000 | 957.66 | 1.70 | | |

| | | | | | | | |
|-------------|------|---------|---|-----|-------|-------|-------|
| S | 0.63 | 1524.65 | 1 | 914 | 0.000 | 6.77 | -0.56 |
| Growth | 0.64 | 1641.32 | 1 | 914 | 0.000 | 3.52 | 4.29 |
| Exponential | 0.64 | 1641.32 | 1 | 914 | 0.000 | 33.79 | 4.29 |
| Logistic | 0.64 | 1641.32 | 1 | 914 | 0.000 | 0.03 | 0.01 |

The independent variable is NDVI, dependent variable is carbon sequestration per plot.

2.6. Landscape pattern

Observing the characteristics of the main urban area blocks in the Zhengzhou metropolitan area, a grid is constructed using 1800 meters as the unit for block division. **The study area is divided into 1037 grid cells.** Subsequently, landscape pattern indices are calculated for each grid cell individually. Landscape indices quantify landscape pattern information, collectively reflecting the quantity, type, proportion, and spatial form of landscapes. There are many types of landscape pattern indices, and some indices are highly correlated with each other. In other words, although some landscape pattern indices have different names and methods of calculation, their meanings often overlap, and an excess of index choices can lead to confusion in results and decision-making. Considering the correlations between landscape metrics, to avoid potential correlations caused by collinearity, the final selection included **Number of Patch (NP), Mean Patch Size (AREA_MN), Mean of Perimeter-Area Ratio (PARA_MN), Euclidean Nearest Neighbor Distance Distribution (ENN_MN), Contrast-Weighted Edge Density (CWED), Edge Contrast Index Distribution (ECON_MN), Percentage of Like Adjacencies (PLADJ), Interspersion & Juxtaposition Index (IJI), Splitting Index (SPLIT), Patch Richness (PR), and Shannon's Evenness Index (SHEI)** as key indicators to analyze the relationship between landscape patterns and carbon sequestration.

These indicators reflect the main characteristics of urban green space landscape patterns from various aspects (Table 2-6). **Using Fragstats 4.2** (KS Mcgarigal et al., 2002), landscape indices for each patch were extracted at the landscape level, and then the landscape pattern indices of each patch were calculated to explore the changing characteristics of Zhengzhou's landscape patterns and their impact on carbon sequestration.

Table 2-6 Landscape metrics, descriptions, and equations

| Metric (Abbreviation) | Descriptions | Equation |
|------------------------------------------------------|-----------------------------------------------------------------------------------------------------------------------------------------------------------------------------------------------------------------------------------------------------------------------------------------------------------------------------|----------------------------------------------------------------------------------------------------------------|
| Average patch size (AREA_MN) | Average size of landscape patches | $AREA_MN = \frac{\sum_{j=1}^n x_{ij}}{n_{ij}}$ |
| Number of patches (NP) | Number of patches | $NP = n$ |
| Dispersion and juxtaposition indices (IJI) | Calculate the overall dispersion and juxtaposition between patch types, where a value of 0 indicates that patch type i is adjacent to only a few other types, and a value of 100 indicates that the lengths of the neighboring edges of patches are equal, i.e., the probability of neighborhoods between patches is equal. | $IJI = \frac{-\sum_{i=1}^m \sum_{k=i+1}^m [(\frac{e_{ik}}{E}) \cdot \ln(\frac{e_{ik}}{E})]}{\ln(0.5[m(m-1)])}$ |
| Mean of Perimeter-Area Ratio (PARA_MN) | Mean of perimeter to area ratio for all landscape patches. | $PARA = \frac{p_{ij}}{a_{ij}}$ |
| Mean of Euclidean Nearest Neighbor Distance (ENN_MN) | The average distance between each point and its nearest neighbor in the Euclidean space. | $ENN = h_{ij}$ |
| Splitting Index (SPLIT) | Determine the number and size of segmented patches based on the actual cumulative area distribution so that the segmented landscape has the same degree of landscape segmentation as the actual. | $SPLIT = \frac{A^2}{\sum_{i=1}^m \sum_{j=1}^n a_{ij}^2}$ |
| Contrast-weight edge density (CWED) | Used to compare edge density between patches of different area sizes | $CWED = \frac{\sum_{i=1}^m \sum_{k=i+1}^n (e_{ik} \cdot d_{ik})}{A} (10000)$ |
| Percentage of Like Adjacencies (PLADJ) | It measures the proportion of neighboring pixels that share the same land cover type. | $PLADJ = \left(\frac{\sum_{i=1}^m (g_{ii})}{\sum_{i=1}^m \sum_{k=1}^m g_{ik}} \right) (100)$ |

| | | |
|---------------------------------|-----------------------------------------------------------------------------------------------------------------------------------|-------------------------------------------------------------------|
| Patch Richness (PR) | Refers to the number of distinct patches or spatially discrete areas of different land cover types within a landscape. | $PR = m$ |
| Simpson's Evenness Index (SHEI) | It considers both the richness (number of species) and the abundance (relative proportions) of different species. | $SHEI = \frac{-\sum_i^m (P_i \cdot \ln P_i)}{\ln m}$ |
| Edge Contrast Index (ECON_MN) | It quantifies how distinct the boundaries between different land cover types are, providing insight into landscape heterogeneity. | $ECON = \frac{\sum_{k=1}^m (P_{ijk} \cdot d_{ik})}{P_{ij}} (100)$ |

X_{ij} represents the area of each patch;
 n represents the number of patches;
 i represents the total edge length (m) including the setup and patch type i ;
 e_{ik} represents the total length (m) of the landscape edge between patches i and k ;
 m represents the number of patches in the landscape;
 E represents the total length of the edge of the landscape including the background; a_{ij} represents the area of patch ij (m^2);
 A represents the total area of all the landscapes in the region (m^2);
 p_{ij} represents the perimeter of patch ij ;
 P_i represents the proportion of total landscapes in the region accounted for by landscape type i .

2.7. Boosted Regression Trees model

The Boosted Regression Trees (BRT) model, pioneered by Friedman in 2000, represents a significant advancement in machine learning. It builds upon the boosting algorithm's success in enhancing classification trees for binary classification problems, extending its utility to regression tasks. By seamlessly integrating boosting with regression tree techniques, BRT constructs a robust regression model that surpasses traditional linear models in both flexibility and predictive power.

The BRT model has a strong self-learning capability and the ability to handle complex variables. It tolerates collinearity and non-normality among dependent variables III. It can be flexibly

used when there are many dependent variables and the relationships are not clear, providing a relatively direct and clear understanding of the impact and relationships between independent and dependent variables. Due to its binary tree structure, the BRT model does not have variables or T-statistics that signify its significance. However, the relative contribution of independent variables to dependent variables can be judged through the model's optimal fit results. Along with marginal effects, the impact of dependent variables on independent variables can be quantified specifically.

In this study, the implementation of the BRT model was carried out on the R 4.2.1 platform, using software packages such as "gbm", "dismo", "caret", and "brt" developed and adapted by Elith and others. BRT is a supervised machine learning method that requires specification of the learning rate, tree complexity, and bagging fraction. To obtain the model's optimal solution, the learning rate was set to 0.01, 0.005, 0.001, tree complexity to 2-6, and based on previous experience, the bagging fraction was set to 0.5, 0.75. The optimal solutions for each parameter were obtained iteratively during tree model construction and output as the final model, which underwent 10-fold cross-validation. The model measures the importance of factors based on the reduction in the sum of squared residuals of the response variable in the regression tree, normalizing the results to represent the importance of each dependent variable to the independent variables in percentage form, with the total importance summing to 1. **The model evaluates the total variance of latent variables and model residual variance, thus constructing a scientifically based model for exploring factors influencing carbon sequestration.**

3. Result

The results section includes the temporal and spatial variations of carbon storage and landscape indices, their correlation, as well as the explanatory rate of multiple landscape indices as independent variables for carbon sequestration.

3.1. Spatial-temporal dynamics of carbon sequestration in the main urban area of the Zhengzhou metropolitan area

This chapter introduces the spatial and temporal distribution of carbon sequestration in urban green spaces within the Zhengzhou metropolitan area from two perspectives: the overall perspective of the Zhengzhou metropolitan area and the perspective of individual cities within it.

3.1.1. General spatial-temporal dynamics of carbon sequestration

The overall characteristics of carbon sequestration capacity in the built-up areas of the Zhengzhou metropolitan area are shown in Figure 3-1 and Table 3-1. **The total carbon sequestration amounts for the years 2013, 2018, and 2023 are 0.67, 0.76, and 0.85 Kg C/m² yr respectively, indicating a positive growth trend overall.** The carbon sequestration capacity of the built-up areas in the Zhengzhou metropolitan area exhibits significant heterogeneity. The maximum value (MAX) increased from 2.26 in 2013 to 2.78 in 2018, then decreased to 2.57 Kg C/m² yr in 2023. This may suggest that there is an upper limit to the carbon sequestration per unit area, as the maximum value of this indicator cannot exceed this limit regardless of time. The standard deviation (STD) measures the degree of dispersion of data points relative to the mean. In these three years, the standard deviations are 0.43, 0.51, and 0.55 respectively. This indicates that in 2023, the dispersion of data points is higher than in 2013 and 2018, implying a wider range of variations in the data.

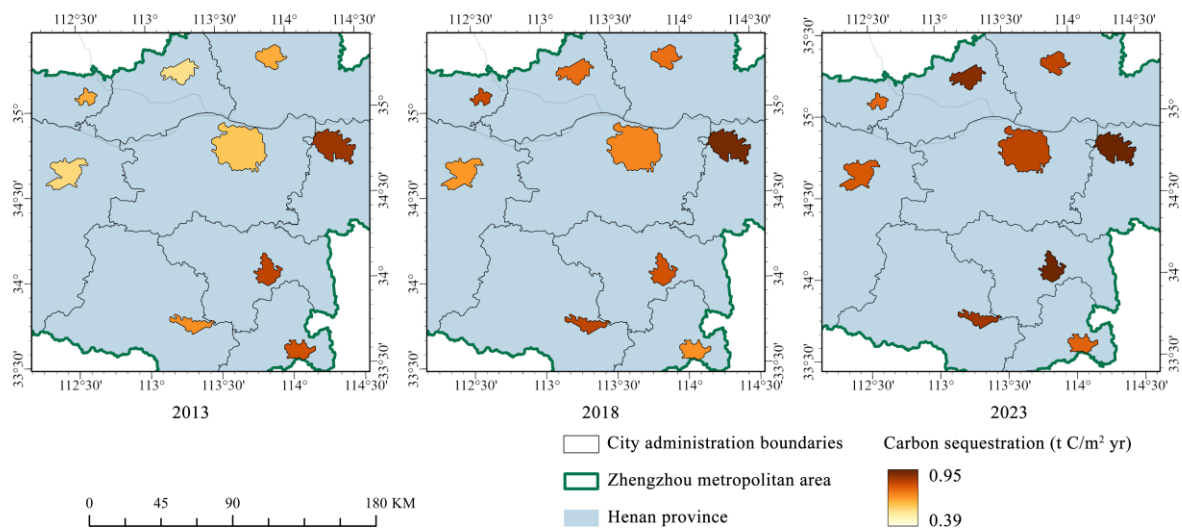
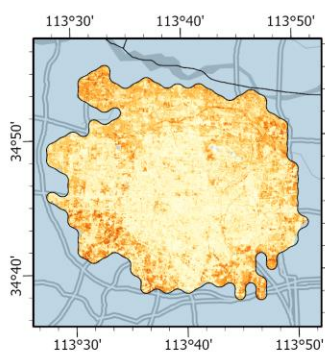


Figure 3-1 Carbon sequestration density of urban green space of Zhengzhou metropolitan area

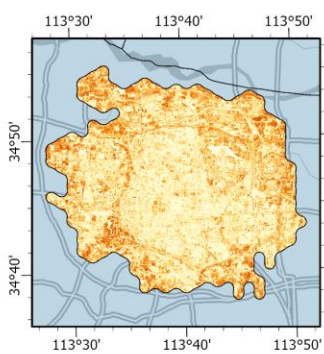
Table 3-1 Carbon sequestration density of urban green space of Zhengzhou metropolitan area (Units: Kg C/m² yr)

| Year | MIN | MAX | RANGE | MEAN | STD | SUM |
|------|-----|------|-------|------|------|------------|
| 2013 | 0 | 2.26 | 2.26 | 0.67 | 0.43 | 1828057.89 |
| 2018 | 0 | 2.78 | 2.78 | 0.76 | 0.51 | 2060769.36 |
| 2023 | 0 | 2.57 | 2.57 | 0.85 | 0.55 | 2320311.68 |

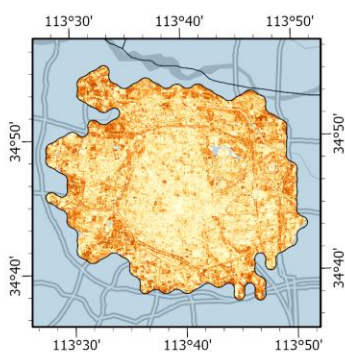
3.1.2. Spatial-temporal dynamics of carbon sequestration between cities



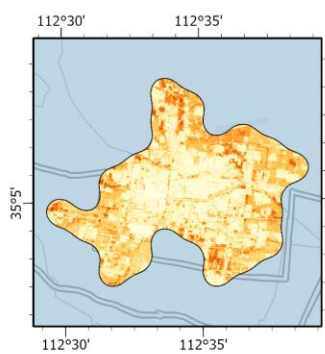
(a1) Zhengzhou 2013 CS



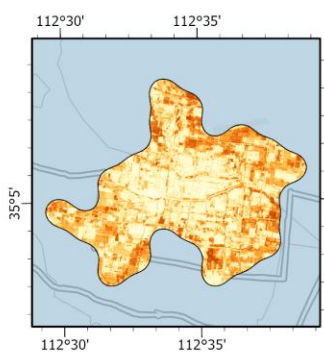
(a2) Zhengzhou 2018 CS



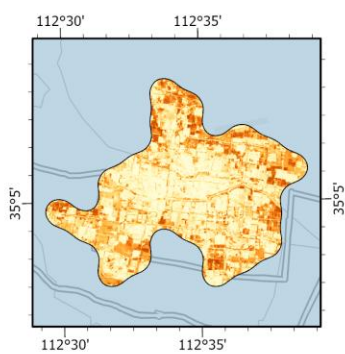
(a3) Zhengzhou 2023 CS



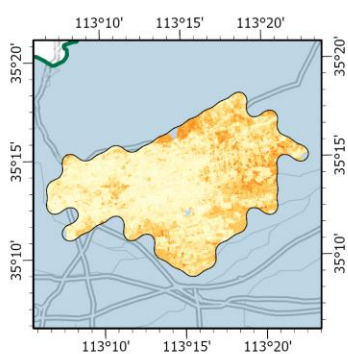
(b1) Jiyuan 2013 CS



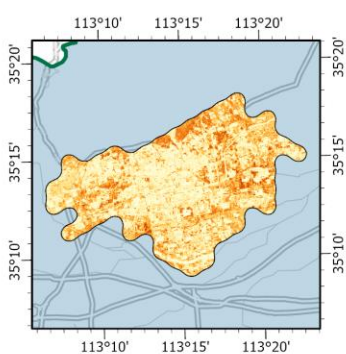
(b2) Jiyuan 2018 CS



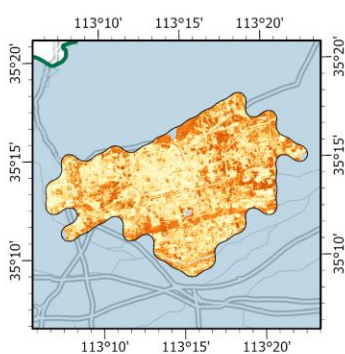
(b3) Jiyuan 2023 CS



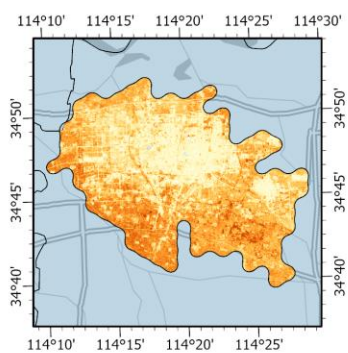
(c1) Jiaozuo 2013 CS



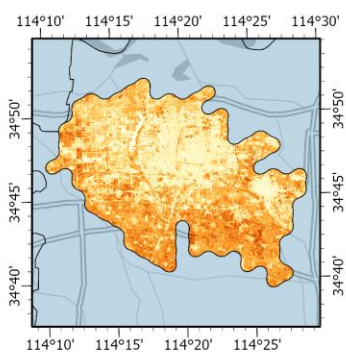
(c2) Jiaozuo 2018 CS



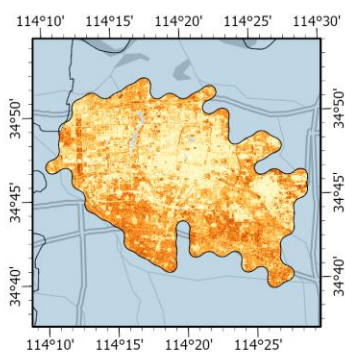
(c3) Jiaozuo 2023 CS



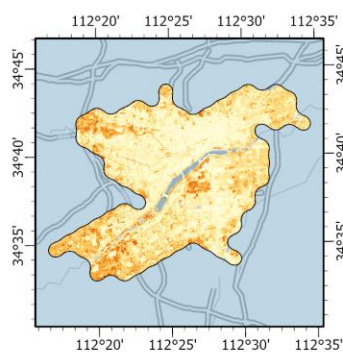
(d1) Kaifeng 2013 CS



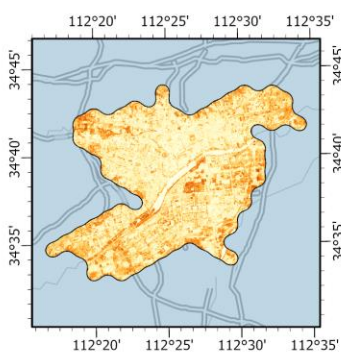
(d2) Kaifeng 2018 CS



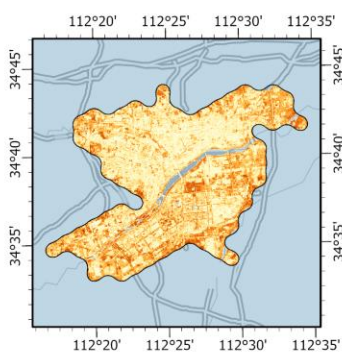
(d3) Kaifeng 2023 CS



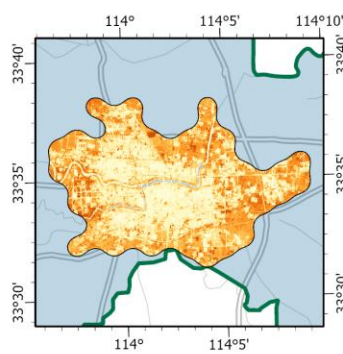
(e1) Luoyang 2013 CS



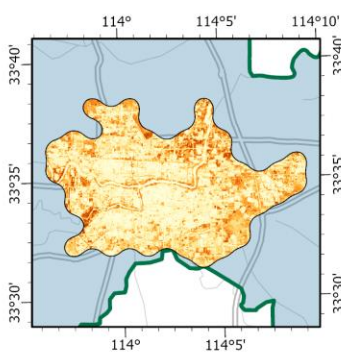
(e2) Luoyang 2018 CS



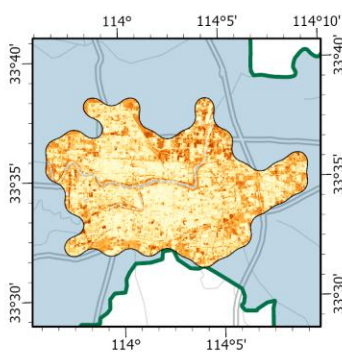
(e3) Luoyang 2023 CS



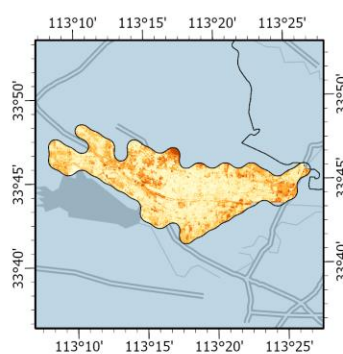
(f1) Luohe 2013 CS



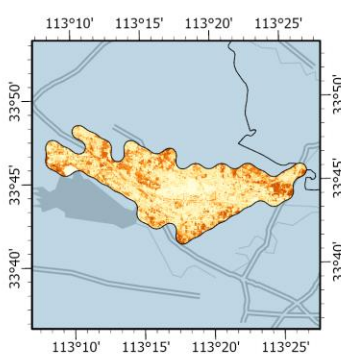
(f2) Luohe 2018 CS



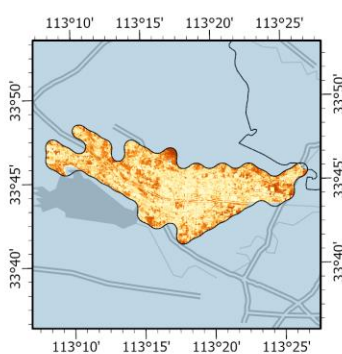
(f3) Luohe 2023 CS



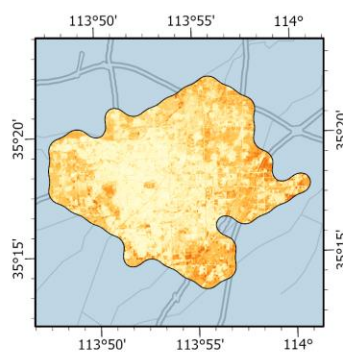
(g1) Pingdingshan 2013 CS



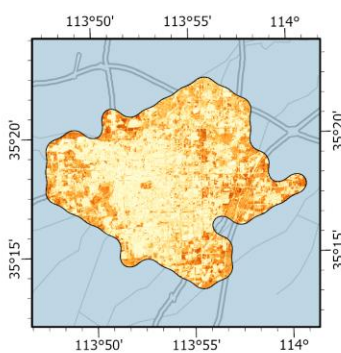
(g2) Pingdingshan 2018 CS



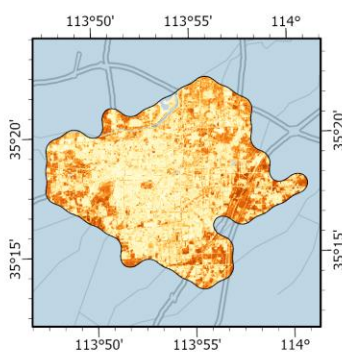
(g3) Pingdingshan 2023 CS



(h1) Xinxiang 2013 CS



(h2) Xinxiang 2018 CS



(h3) Xinxiang 2023 CS

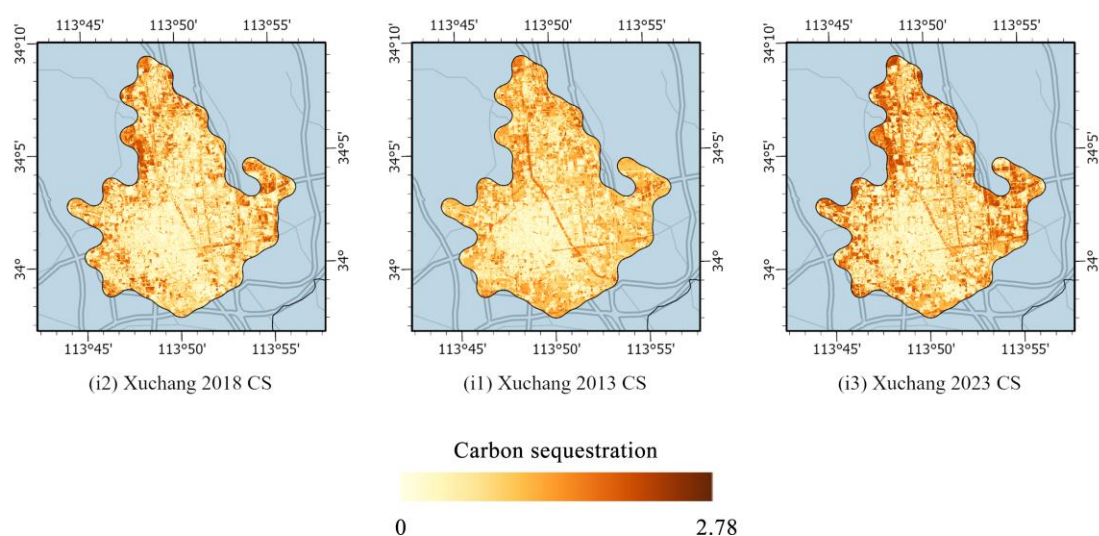


Figure 3-2 Carbon sequestration distribution

Table 3-2 Carbon sequestration distribution

| City | Year | Min | Max | Mean | STD | Sum |
|--------------|------|------|------|------|------|-----------|
| Xinxiang | 2013 | 0.01 | 2.01 | 0.64 | 0.35 | 130461.66 |
| | 2018 | 0.00 | 2.37 | 0.74 | 0.50 | 151557.52 |
| | 2023 | 0.00 | 2.38 | 0.83 | 0.56 | 168074.29 |
| Pingdingshan | 2013 | 0.00 | 2.18 | 0.69 | 0.42 | 116237.92 |
| | 2018 | 0.00 | 2.78 | 0.83 | 0.55 | 126114.33 |
| | 2023 | 0.00 | 2.42 | 0.87 | 0.56 | 145637.49 |
| Luoyang | 2013 | 0.00 | 2.08 | 0.55 | 0.40 | 181911.68 |
| | 2018 | 0.00 | 2.49 | 0.67 | 0.45 | 226998.17 |
| | 2023 | 0.00 | 2.50 | 0.79 | 0.52 | 258950.33 |
| Jiyuan | 2013 | 0.00 | 2.01 | 0.64 | 0.42 | 59630.44 |
| | 2018 | 0.00 | 2.31 | 0.81 | 0.53 | 75390.94 |
| | 2023 | 0.00 | 2.34 | 0.76 | 0.52 | 70047.03 |
| Jiaozuo | 2013 | 0.00 | 1.83 | 0.54 | 0.34 | 127365.99 |
| | 2018 | 0.00 | 2.34 | 0.75 | 0.50 | 177406.23 |
| | 2023 | 0.00 | 2.35 | 0.90 | 0.56 | 213629.02 |
| Luohe | 2013 | 0.00 | 2.21 | 0.80 | 0.49 | 143536.84 |
| | 2018 | 0.00 | 2.35 | 0.69 | 0.49 | 123750.87 |

| | | | | | | |
|-----------|------|------|------|------|------|-----------|
| | 2023 | 0.00 | 2.48 | 0.77 | 0.52 | 136632.10 |
| | 2013 | 0.00 | 2.21 | 0.83 | 0.46 | 182422.53 |
| Xuchang | 2018 | 0.00 | 2.63 | 0.80 | 0.54 | 170426.94 |
| | 2023 | 0.00 | 2.48 | 0.94 | 0.59 | 206572.21 |
| | 2013 | 0.00 | 2.22 | 0.59 | 0.41 | 514769.62 |
| Zhengzhou | 2018 | 0.00 | 2.52 | 0.70 | 0.52 | 615288.41 |
| | 2023 | 0.00 | 2.57 | 0.83 | 0.56 | 722125.36 |
| | 2013 | 0.00 | 2.26 | 0.88 | 0.45 | 371721.21 |
| Kaifeng | 2018 | 0.00 | 2.35 | 0.93 | 0.50 | 393835.95 |
| | 2023 | 0.00 | 2.41 | 0.94 | 0.51 | 398643.85 |

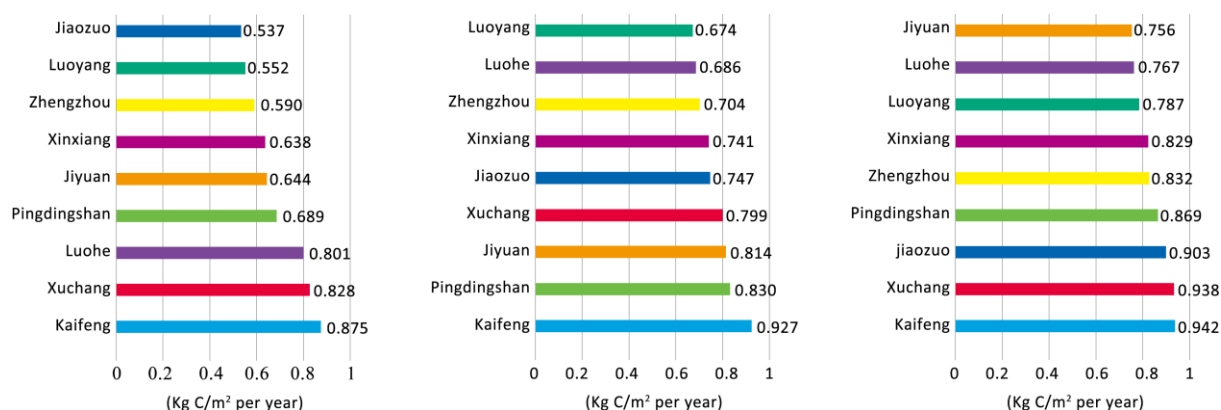


Figure 3-3 Compare carbon sequestration in different cities (from left to right in 2013, 2018, and 2023).

As shown in Figures 3-2, 3-3, and Table 3-2, there is significant spatial variation in the carbon sequestration capacity of the built-up areas in the Zhengzhou metropolitan area. Kaifeng City consistently leads in green space carbon sequestration capacity among the other eight cities, and it has shown a consistently increasing trend, reaching 0.94 Kg C/m² yr for all cities in 2023. Xinxiang, Pingdingshan, Luoyang, Jiaozuo, and Zhengzhou city have also shown continuous growth over the past 10 years, but with significantly different growth rates. Among them, Jiaozuo city has the largest increase, with a carbon storage increase of 0.37 Kg C/m² yr over the past decade, followed by Zhengzhou and Luoyang cities, both with an increase of 0.24 Kg C/m² yr, while Pingdingshan and Xinxiang cities are in the third tier, with increases of 0.18 and

0.18 Kg C/m² yr, respectively. Kaifeng city has the lowest increase, at only 0.07 Kg C/m² yr.

In contrast, the urban green spaces in Jiyuan city initially showed an increase followed by a decrease, while Luohe and Xuchang cities showed a decrease followed by an increase. Although the carbon storage of urban green spaces in Jiyuan and Xuchang cities fluctuated over the past 10 years, they both increased by 0.11 Kg C/m² yr overall during this period. However, in 2023, Jiyuan City still had the lowest carbon sequestration capacity for urban green spaces, with a mean of 0.76 Kg C/m² yr. Luohe City is the only city that showed a decline in urban green space carbon sequestration over the past 10 years, decreasing by 0.03 Kg C/m² yr.

3.2. Characteristics of spatio-temporal differentiation of landscape pattern

Landscape indices, including Shannon's Evenness Index (SHEI), Patch Richness (PR), Edge Contrast Index Distribution (ECON_MN), Contrast-weight Edge Density (CWED), Perimeter-Area Ratio Distribution (PARA_MN), Mean of Patch Area Distribution (AREA_MN), Number of patches (NP), Euclidean Nearest Neighbor Distance Distribution (ENN_MN), Splitting Index (SPLIT), Percentage of Like Adjacencies (PLADJ), and Interspersion & Juxtaposition Index (IJI), exhibited notable differences across various years (Figure 3-4 and Table 3-3).

SHEI and PR, both diversity metrics, demonstrated distinct characteristics. SHEI quantifies diversity relative to the maximum possible diversity, while PR measures the number of patch types irrespective of their relative abundance or spatial arrangement. Despite different landscape structures, two landscapes may possess identical richness values. SHEI values ranged from 0 to 1, with mean values of 0.61, 0.60, and 0.51 for 2013, 2018, and 2023, respectively. As the index grows, it exhibits a more even representation of different landscape types. PR values ranged from 1 to 5, with most patches containing 3-4 land use types (without cropland in urban areas).

ECON_MN and CWED, contrast metrics, highlighted differences in adjacent patch types at specific scales. ECON_MN represented the average edge contrast across all patches, showing

significant increase and distribution disparities over time, with a mean value of 61.80 in 2023, and 1.49 times the mean value of 41.52 in 2013. CWED shows a similar growth trend from 47.52 in 2013 to 61.64 in 2023. This indicates that the urbanization process in the Zhengzhou metropolitan area has resulted in an increasingly clear delineation of the nature of land use and the strengthening of land use attributes.

PARA_MN peaked at 948.21 in 2018, while the dispersion of the index has been increasing from 2013-2023, with the STD value growing from 93.49 in 2013 to 100.57 in 2023. The mean value of AREA_MN was the smallest, but the dispersion value was the largest in 2018 (3.14) as compared to other years. This is a side effect of the fact that the city's landscape patches have undergone a round of reconstruction over time, which is also consistent with reality.

Aggregate indicators NP, ENN_MN, SPLIT, PLADJ, and IJI also exhibit distinct trends. The average value of ENN_MN fluctuates minimally in 2013, 2018, and 2023, maintaining relative stability. Meanwhile, NP and SPLIT have demonstrated similar developmental trajectories over the past decade, characterized by initial growth followed by decline. NP measures the number of landscape patches, while SPLIT assesses the fragmentation degree of the landscape. Due to increased landscape fragmentation, the quantity of landscape patches inevitably increases. The congruent trends of these two indices are comprehensible. The mean value of the SPLIT index reached its lowest point in the past decade in 2023, at 2.42. Concurrently, its standard deviation also reaches its nadir, indicating that the overall Zhengzhou metropolitan area is entering the later stages of urbanization, with urban morphology trending towards stability.

Table 3-3 Statistic of landscape metrics

| Landscape indices | Average | | | STD | | |
|-------------------|---------|--------|--------|-------|-------|--------|
| | 2013 | 2018 | 2023 | 2013 | 2018 | 2023 |
| NP | 64.30 | 66.91 | 50.94 | 36.03 | 21.21 | 25.75 |
| AREA_MN | 4.23 | 3.90 | 4.91 | 2.81 | 3.14 | 2.39 |
| PARA_MN | 934.29 | 948.21 | 933.94 | 93.49 | 97.49 | 100.57 |
| ENN_MN | 111.26 | 110.82 | 126.98 | 44.07 | 39.23 | 52.89 |

| | | | | | | |
|---------|-------|-------|-------|-------|-------|-------|
| CWED | 47.52 | 55.12 | 61.64 | 32.98 | 23.52 | 31.24 |
| ECON_MN | 41.52 | 55.34 | 61.80 | 16.59 | 11.71 | 20.12 |
| PLADJ | 81.29 | 89.69 | 83.61 | 7.95 | 6.95 | 7.97 |
| IJI | 59.44 | 49.71 | 48.82 | 15.75 | 12.37 | 19.91 |
| SPLIT | 3.18 | 4.01 | 2.42 | 2.01 | 2.41 | 1.40 |
| PR | 3.86 | 3.40 | 4.18 | 0.74 | 0.77 | 0.80 |
| SHEI | 0.61 | 0.60 | 0.51 | 0.20 | 0.17 | 0.20 |

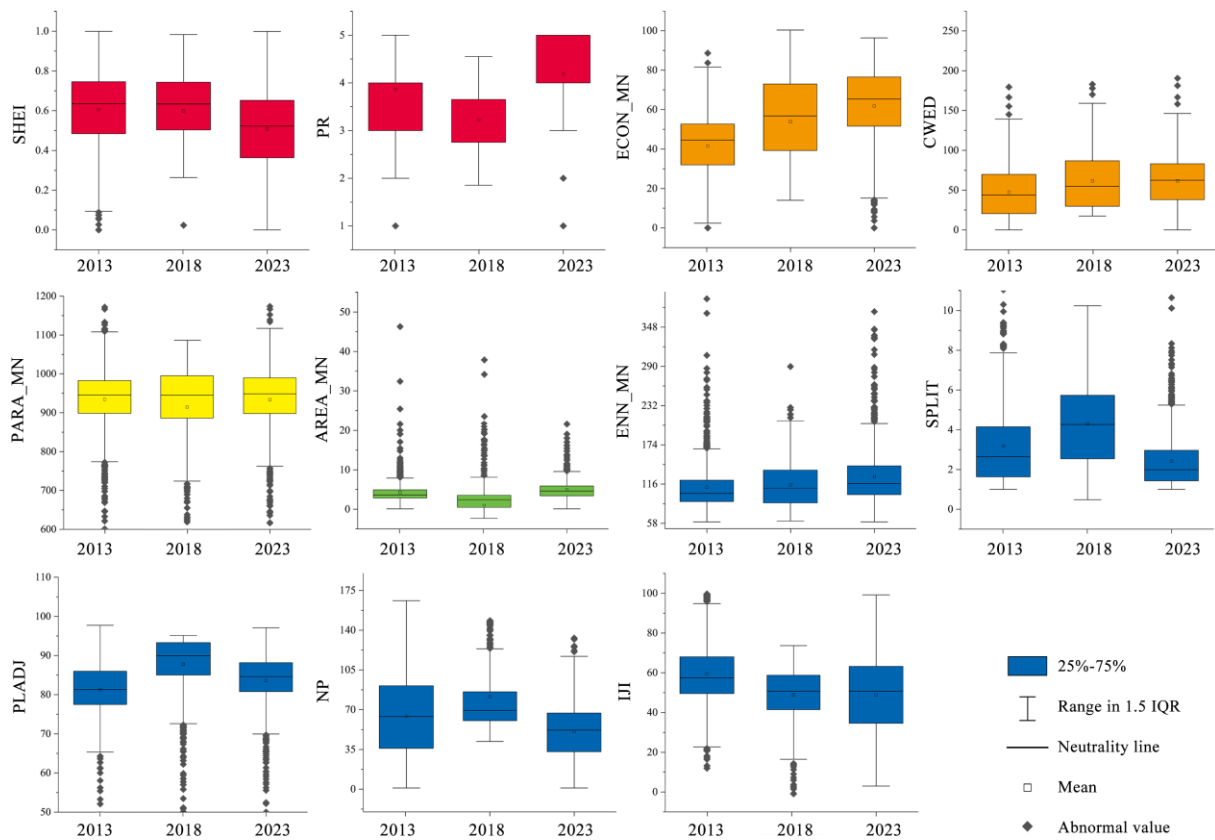


Figure 3-4 Landscape metrics value

3.3. Correlation analysis between landscape pattern and urban carbon sequestration

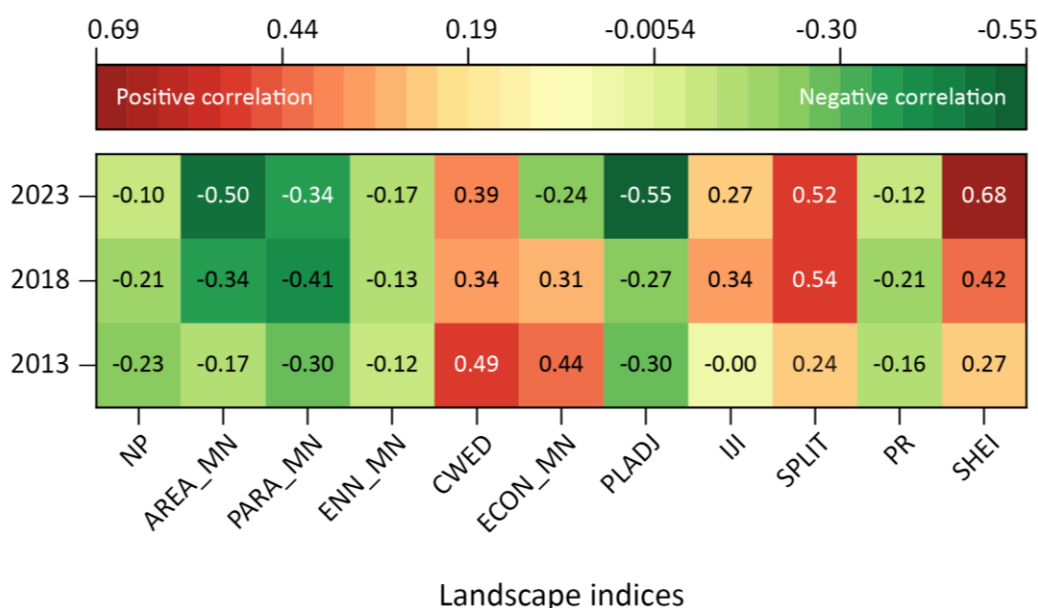


Figure 3-5 Correlation analysis between carbon sequestration and landscape pattern

To ensure that there is no significant multicollinearity among landscape indices, multicollinearity tests were conducted among them, with all variance inflation factor (VIF) values being less than 5, indicating no evident multicollinearity among the landscape indices. Figure 3-5 depicts the results of Pearson correlation analysis between carbon sequestration density and various landscape indices. **Overall, carbon sequestration is significantly correlated with landscape indices across all years, and the overall trends are generally similar.** Furthermore, as the years progress, the strength of the correlation between carbon sequestration and several landscape indices shows an increasing trend, including AREA_MN, ENN_MN, PLADJ, and SHEI, among others. This systematic change may be related to the urbanization process. **CWED, IJI, SPLIT, and SHEI exhibit positive correlations with carbon sequestration; NP, AREA_MN, PARA_MN, ENN_MN, PLADJ, and PR exhibit negative correlations with carbon sequestration;** the correlation between ECON_MN and carbon sequestration is negative in 2023, while it is positive in 2018 and 2013, possibly due to a critical threshold point in the correlation between ECON_MN and carbon sequestration.

In 2013, CWED (0.49) and ECON_MN (0.44) showed the strongest correlations with carbon sequestration, both positively correlated; PARA_MN and PLADJ also exhibit significant negative correlations with carbon sequestration (correlations of 0.30 each). In 2018, SPLIT and

SHEI showed strong positive correlations with carbon sequestration, with correlations of 0.54 and 0.42, respectively. PARA_MN exhibits a significant negative correlation, with a correlation of -0.41. In 2023, the correlation between carbon sequestration and landscape indices is particularly evident, with correlations greater than 0.5 with AREA_MN, PLADJ, SPLIT, and SHEI. Specifically, positive correlations are observed with SPLIT and SHEI, while negative correlations are observed with AREA_MN and PLADJ.

3.4. Relative contribution of landscape pattern indices to carbon sequestration

The decision tree regression parameter settings are shown in Table 3-4, with all samples used for constructing the training set. The model evaluation results for the years 2013, 2018, and 2023 are presented in Table 3-5. The model results indicate that the relative importance predictions have a good explanatory power.

Table 3-4 Setting Parameters of Decision Regression Tree

| Parametric | Value |
|-------------------------------------------------------------------|--------------|
| Data slicing | 1 |
| Data shuffling | disable |
| Cross-validation | disable |
| Node splitting criterion | friedman_mse |
| Feature split point criterion | best |
| The minimum number of samples required to split an internal node | 2 |
| The minimum number of samples required to be at a leaf node | 1 |
| The minimum weight fraction of the sum of weights | 0 |
| The maximum depth of the tree | 10 |
| The maximum number of leaf nodes | 50 |
| The threshold impurity for node splitting | 0 |
| The maximum proportion of features to be considered when dividing | None |

Table 3-5 Results of the model evaluation

| YEAR | MSE | RMSE | MAE | MAPE | R ² |
|------|-----|------|-----|------|----------------|
|------|-----|------|-----|------|----------------|

| | | | | | |
|------|-------|-------|-------|--------|-------|
| 2023 | 0.018 | 0.135 | 0.105 | 11.971 | 0.768 |
| 2018 | 0.018 | 0.129 | 0.101 | 12.451 | 0.689 |
| 2013 | 0.019 | 0.137 | 0.102 | 15.377 | 0.761 |

In 2013, the CEWD index exhibited the highest relative explanatory power for urban green space carbon sequestration in the Zhengzhou metropolitan area, reaching 30%, far surpassing other indices. SPLIT, PARA_MN, and NP also contributed significantly to explaining carbon sequestration in 2013, with explanatory powers exceeding 10% each, reaching 17%, 15%, and 13%, respectively. In 2018, the IJI and SHEI indices play a predominant explanatory role, with explanatory powers of 29% and 22%, respectively. Additionally, NP, AREA_MN, and CWED also contribute to explaining variations in green space carbon sequestration. In 2023, the SPLIT index demonstrates an explanatory power of 55% for carbon sequestration, while the SHEI index also provides some explanation for changes in carbon sequestration.

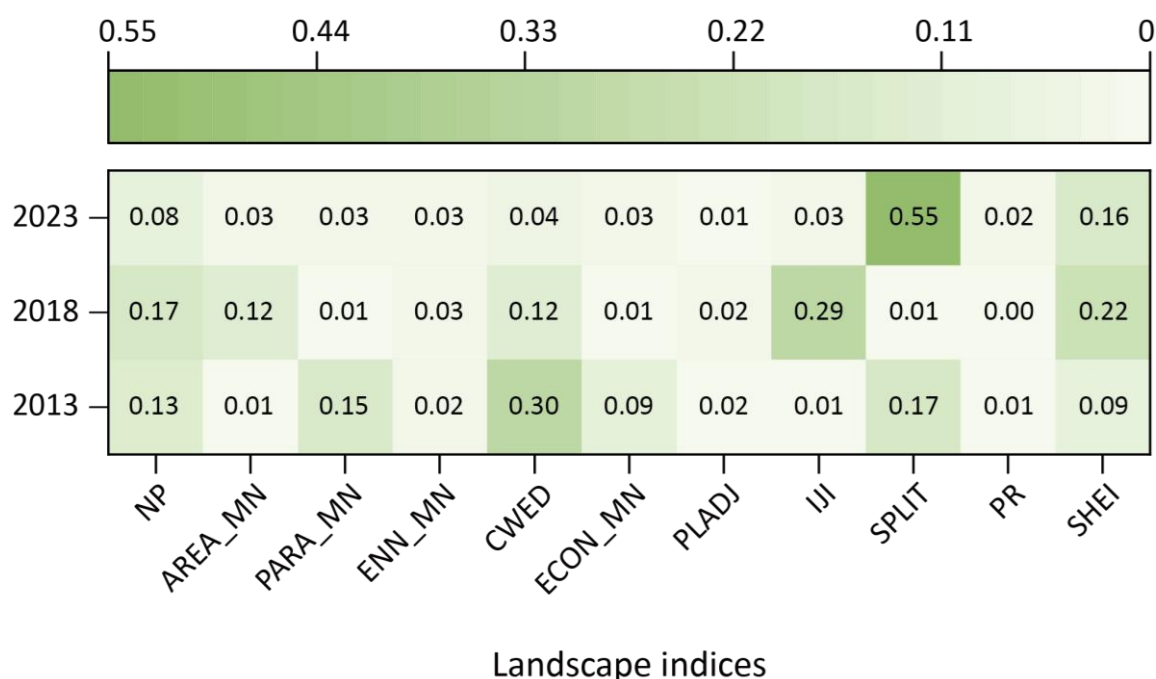


Figure 3-6 Relative contribution of landscape pattern indices to carbon sequestration

4. Discussion

This chapter discusses urban carbon sequestration, the impact of landscape patterns on urban

carbon sequestration, and measures proposed based on the results of this study to enhance the efficiency of urban carbon sequestration in urban green spaces.

4.1. Carbon sequestration changes in urban green spaces

The carbon sequestration capacity of urban green spaces has been confirmed in studies conducted at various scales. Some studies have focused on urban parklands and forests. For instance, (Y. Wang et al., 2021) indicated in their 2021 study that the carbon sequestration benefits of 25 urban parks in Beijing were 2.06 kg C /m² yr. Similarly, (Jia et al., 2023) conducted a study on specific urban parklands and determined that the carbon storage of the China Green Expo Park was 30.72 kg/m². These research findings exhibit significant disparities compared to the results of my study, which can be attributed to the significantly higher biomass of vegetation in urban parks compared to overall urban green spaces, a factor which is not discussed in this paper.

Taking urban green spaces as a whole, numerous studies have investigated the carbon sequestration and storage of urban green spaces at different scales. My research findings indicate that the carbon sequestration in the Zhengzhou metropolitan area was 0.67 kg C /m² yr in 2013, 0.67 kg C /m² yr in 2018, and 0.85 kg C /m² yr in 2023. As different studies were conducted in different years, I compared my data with those closest in proximity. A study on multiple major cities in South Korea revealed average carbon absorption and carbon storage densities of 0.26 kg C /m² yr and 2.99 ± 0.17 kg C /m², respectively, capable of offsetting 1.5% of residential energy consumption (Jo et al., 2023). In 2013, the carbon sequestration in the Zhengzhou metropolitan area was 0.67 kg C /m² yr, which is much higher than a study conducted in the United States in the same year, where urban whole tree carbon storage densities averaged 7.69 kg C m⁻² of tree cover, and sequestration densities averaged 0.28 kg C /m² of tree cover per year. In 2007, a study on urban green spaces in Zhengzhou City suggested that the carbon storage and sequestration were 1.9 kg C /m² yr and 0.29 kg C /m² yr, respectively (W. Y. Chen, 2015). A study conducted in Shenyang, China, in 2012 reported that the carbon sequestration of urban green spaces in Shenyang was 0.28 kg C /m² yr (Liu & Li, 2012). A study on urban forests in Hangzhou, China, in 2010 indicated a carbon sequestration

of 0.17 kg C /m² yr and a carbon storage of 3.03 kg C /m². Another study in Beijing in 2010 found that the carbon sequestration and storage of urban green spaces were 0.22 kg C /m² yr and 1.93 kg C /m², respectively (J. Zhao et al., 2010). Another study conducted in the same research area of Beijing in 2019 revealed an increase in the carbon storage of urban green spaces to 7.8 kg C /m² (Sun et al., 2019). Combining the results of these two studies, it can be indirectly inferred that the carbon sequestration of urban green spaces in Beijing is experiencing rapid growth, consistent with the findings of my study. (Escobedo et al., 2010) conducted a study on urban forests in a city in Florida, indicating that urban trees sequestered 3.4% and 1.8% of the total emissions of Gainesville city and Miami-Dade city, respectively.

4.2. Landscape drivers of carbon sequestration capacity in urban green spaces

In recent years, numerous scholars have undertaken research aimed at promoting carbon sequestration in urban green spaces. (Y. Wang et al., 2021) mentioned promoting carbon sequestration efficiency in urban green spaces through plant design, and studying differences in carbon sequestration efficiency among individual plants and different plant communities. (Jo et al., 2023) suggested several planting strategies to boost carbon storage efficiency in urban parks. These include trimming unnecessary grassland and sidewalk areas, strategically planting trees in available spaces, adopting multi-layered planting approaches, and opting for fast-growing tree species.

In previous studies, the correlation between carbon sequestration in urban green spaces and landscape patterns has been repeatedly confirmed (N. Shi et al., 2024). Research on Xiamen City indicated that SHDI was significantly positively correlated with vegetation carbon density at the class level ($P < 0.01$), making it the most sensitive landscape index to carbon storage (Hua, 2013). (Sun et al., 2019) found in their 2019 study that PLAND and AI showed a positive correlation with carbon storage density, while ENN_MN showed a negative correlation, consistent with the results of my study. Similarly, a study in Nanjing in 2023 also showed a positive correlation between carbon sequestration and PLAND and AI but a negative correlation with DIVISION and LSI. A study conducted in China found that lower landscape heterogeneity and fragmentation, along with a decreased concentration of urban built-up land,

contribute to carbon reduction. Conversely, decreasing landscape complexity and connectivity would lead to increased carbon emissions (Tang et al., 2023). A study on wetlands in Wuhan City indicated that TA, LSI, SHDI, and AI were all positively correlated with carbon sequestration in Wuhan wetlands, with correlation coefficients all exceeding 0.3. However, PD and LPI were negatively correlated with carbon storage in the study area (Song et al., 2023).

4.3. Regulatory strategies based on carbon sinks in urban green spaces.

This paper seeks to explain the variations in urban green space carbon sequestration through landscape patterns and proposes strategies to enhance urban green space carbon sequestration by adjusting these patterns. Firstly, it must be acknowledged that the differences in correlation and explanatory power between landscape indices and urban carbon sequestration across different years are significant. This is because changes in urban green space carbon sequestration are influenced by multiple factors, with landscape patterns being just one significant driving factor that cannot fully account for all variations in urban green space carbon sequestration. This argument will be elaborated further in Section 5.3. Secondly, the analysis of explanatory power compares the relative importance of 11 landscape indices in explaining carbon sequestration in the Zhengzhou metropolitan area for a given year. When a certain index exhibits a significant correlation with carbon sequestration for a particular year and has relatively high explanatory power, I believe that changes in this index can provide guidance for enhancing urban green space carbon sequestration. Based on the research results on the correlation and explanatory power between urban green space carbon sequestration and landscape indices in the Zhengzhou metropolitan area, three strategies have been derived.

In 2013, CWED exhibited the highest explanatory power at 30%, while showing a significant positive correlation of 0.49 with urban green space carbon sequestration. This indicates that, for landscape patches themselves, the complexity of patch shape edges can positively influence the carbon sequestration efficiency of urban green spaces. **By increasing the complexity of landscape patch shapes, the overall carbon sequestration efficiency of the landscape can be enhanced (see Figure 4-1a).** It is worth noting that PARA_MN index

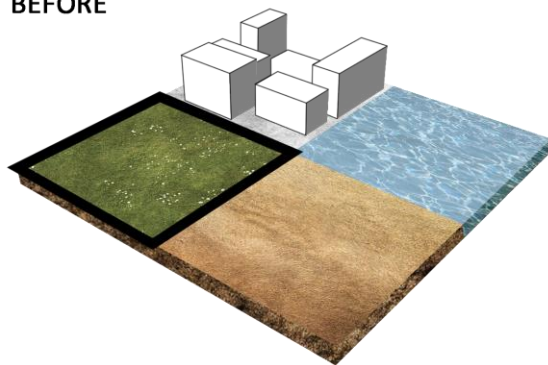
represents the ratio of perimeter to area of landscape patches, similarly reflecting the complexity of patch shapes, but its calculation is influenced by the size of landscape patches. Although PARA_MN also shows a strong correlation with urban green space carbon efficiency, its explanatory power for carbon efficiency is significantly lower than CWED. This indirectly demonstrates that the size of landscape patches significantly influences urban carbon sequestration.

In 2018, the IJI index provides more explanation for the distribution variability of carbon sequestration, with a correlation of 0.34. The IJI index characterizes the spatial relationships between landscape patches, reaching its maximum value when a landscape patch is adjacent to multiple different types of patches with equal contact area. This may be due to the exchange of elements in the atmosphere between different patches, thereby promoting photosynthesis in plants. For instance, research by (Weissert et al., 2017) indicates that higher nitrogen concentration can enhance carbon sequestration efficiency in plants. In the same year, the SHEI index also played a strong explanatory role in carbon sequestration, once again confirming that the uniform distribution of different types of patches can enhance the carbon sequestration efficiency of urban green spaces. Therefore, **enhancing connectivity between different landscape patches and maximizing the equality of contact area with other patches can improve the overall carbon sequestration efficiency of the landscape (see Figure 4-1b).**

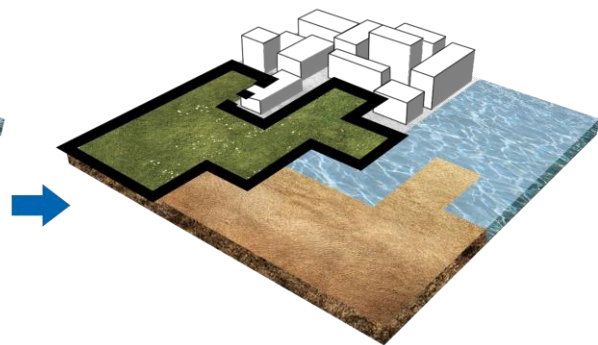
In 2023, SPLIT demonstrates an explanatory power of 55% for carbon sequestration, showing a significant positive correlation of 0.52 with carbon sequestration. This suggests that urban planning can promote urban green space carbon sequestration by **reducing the distance between different streets, thereby facilitating the fragmentation of urban blocks (see Figure 4-1c).** The author speculates that this is because a more dispersed land layout may be more conducive to the formation and development of green spaces, thereby increasing urban green space carbon sequestration.

(a) Strategy 1

BEFORE

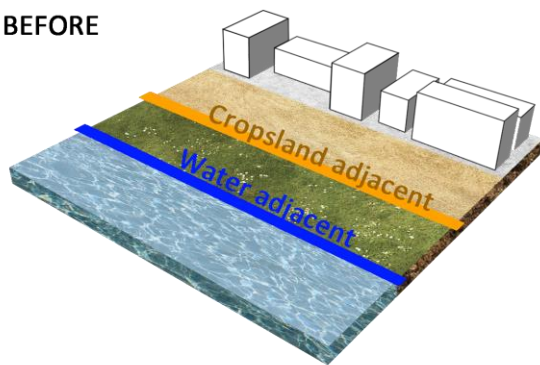


IMPROVED

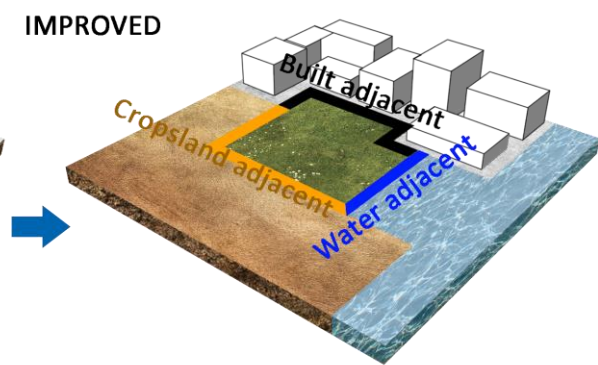


(b) Strategy 2

BEFORE

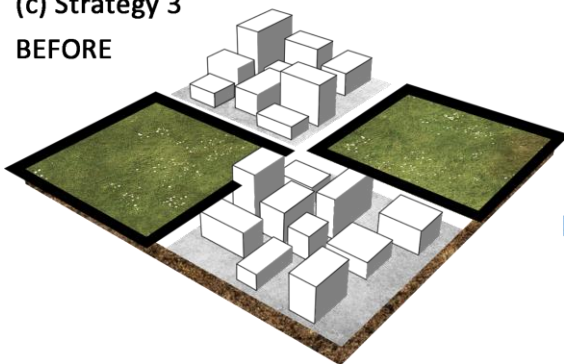


IMPROVED



(c) Strategy 3

BEFORE



IMPROVED

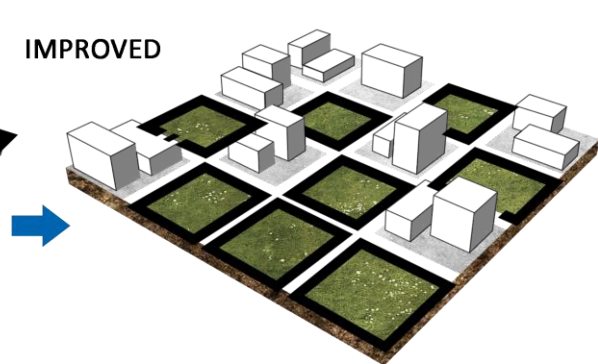


Figure 4-1 Strategies for increasing carbon sequestration

5. Conclusion

The conclusion section summarizes the research findings of the thesis, discusses its limitations, and outlines prospects for future research.

5.1. Research Results

This study conducted field surveys on a total of 974 plots, each measuring 20×20 meters, within nine cities including Zhengzhou metropolitan area, to investigate vegetation growth conditions. By combining the NDVI values of the study area, a relationship model between NDVI and carbon sequestration was established to estimate the carbon sequestration of the main urban areas in the nine cities of the Zhengzhou metropolitan area. The study area was divided into grids, and 11 landscape indices were calculated at the landscape level using Fragstats software. The correlation between carbon sequestration and landscape indices of each grid was analyzed. Based on landscape patterns, strategies to enhance carbon sequestration in urban green spaces were proposed. The results indicate that landscape indices CWED, SPLIT, and SHEI exhibit strong positive correlations with carbon sequestration, while NP, AREA_MN, PARA_MN, PLADJ, and carbon sequestration show strong negative correlations. Based on the explanatory rate of these indices on urban green space carbon sequestration, it is concluded that in urban planning, reducing the size of blocks to a certain extent is beneficial for the formation of urban green space patches. Simultaneously, it is recommended to intersperse functional zones of different land use types to increase the contiguity and average contact of a land use patch with other patches of different land use types.

5.2. Research Shortcomings

This study explores urban planning strategies conducive to enhancing the carbon sequestration benefits of urban green spaces by examining the correlation between urban green space carbon storage and landscape patterns in 2013, 2018, and 2023. **A 5-year time slice** was selected to observe changes in carbon sequestration and landscape patterns. Due to rapid urban development and frequent land use changes, the coherence and heterogeneity of the research results cannot be fully demonstrated, leading to considerable uncertainty.

The use of grid-based division for urban built-up areas, as employed in this study, to construct landscape patches lacks practical significance. In subsequent research, **alternative methods such as dividing landscape patches based on urban functional blocks could be considered.**

For example, (Hong et al., 2024) divided built-up areas into large, medium, and small categories based on population, into low, medium, and high categories based on elevation, and into different degrees of newness based on construction time.

Moreover, landscape index analysis generally involves three levels: patch, class, and landscape. This study focused on the landscape level for analysis, taking a macroscopic perspective on the impact of landscape patterns on urban green space carbon sequestration, without excluding the contributions of cropland, built-up land, and water bodies to carbon sequestration. To provide a more accurate description of the role of urban green spaces, **efforts could be made to eliminate the influence of land use types other than green spaces on carbon sequestration and to conduct landscape pattern analysis based on green space categories.**

5.3. Research Prospects

Factors influencing carbon sequestration benefits of urban green spaces are diverse. For instance, (Lin et al., 2023) analyzed socio-economic factors including total population, per capita GDP, the proportion of urban green spaces, urban built-up area size, the proportion of secondary industry value, and the proportion of primary industry value, as well as climate factors such as NDVI, average annual climate, annual mean potential evapotranspiration, and annual mean solar radiation. (Hong et al., 2024) studied the Changchun urban agglomeration in China and selected six anthropogenic indicators including urban area, urban development intensity, building height, compactness, road network density, population density, and GDP, along with four natural indicators including NDVI, annual mean precipitation, annual mean potential evapotranspiration, and surface temperature. In a large-scale study in Guangxi Province, China, (Guo et al., 2023) identified NDVI, nighttime light index (NLI), GDP, and population density as driving factors. Soil nitrogen content and species diversity index were observed as primary drivers in a study on mangrove carbon storage (Meng et al., 2022). In a cloud-based urban carbon footprint study (Shang & Luo, 2021), factors driving carbon footprint changes were categorized into urban size, economic development, social systems, and technological progress.

Based on this, in further research, establishing a database of driving factors for urban green space carbon sequestration and comprehensively evaluating the roles of various driving factors could be considered. Additionally, considering different development scenarios and simulating optimal urban green space system planning strategies based on carbon neutrality concepts and urban planning schemes (Ernst et al., 2022) would be beneficial. (D. Guan et al., 2023) considered 16 driving factors including economic, natural, and social aspects in their study of Chongqing, China, and simulated four scenarios, demonstrating that forest area, DEM, and tree age were the primary drivers affecting urban forest carbon sequestration efficiency. (M. Shi et al., 2022) designed three different land use development scenarios for Xinjiang, China: rapid economic development, ecological land protection, and sustainable development, compared with the current land use development scenario. The results showed that the sustainable development scenario had the smallest gap between carbon demand and supply, which was more consistent with local development. In future research, combining landscape architecture with urban planning and adjusting landscape patterns based on research results could be attempted to set different land use development scenarios, exploring scenarios more conducive to enhancing urban carbon sequestration.

Reference

- Almanza, E., Jerrett, M., Dunton, G., Seto, E., & Ann Pentz, M. (2012). A study of community design, greenness, and physical activity in children using satellite, GPS and accelerometer data. *Health & Place*, 18(1), 46–54. <https://doi.org/10.1016/j.healthplace.2011.09.003>
- Ambrey, C., & Fleming, C. (2014). Public Greenspace and Life Satisfaction in Urban Australia. *Urban Studies*, 51(6), 1290–1321. <https://doi.org/10.1177/0042098013494417>
- Arneth, A., Sitch, S., Pongratz, J., Stocker, B. D., Ciais, P., Poulter, B., Bayer, A. D., Bondeau, A., Calle, L., Chini, L. P., Gasser, T., Fader, M., Friedlingstein, P., Kato, E., Li, W., Lindeskog, M., Nabel, J. E. M. S., Pugh, T. A. M., Robertson, E., ... Zaehle, S. (2017). Historical carbon dioxide emissions caused by land-use changes are possibly larger than assumed. *Nature Geoscience*, 10(2), 79–84. <https://doi.org/10.1038/ngeo2882>
- Beer, C., Reichstein, M., Tomelleri, E., Ciais, P., Jung, M., Carvalhais, N., Rödenbeck, C., Arain, M. A., Baldocchi, D., Bonan, G. B., Bondeau, A., Cescatti, A., Lasslop, G., Lindroth, A., Lomas,

- M., Luyssaert, S., Margolis, H., Oleson, K. W., Rouspard, O., ... Papale, D. (2010). Terrestrial Gross Carbon Dioxide Uptake: Global Distribution and Covariation with Climate. *Science*, 329(5993), 834–838. <https://doi.org/10.1126/science.1184984>
- Cai, B., Wang, X., Huang, G., Wang, J., Cao, D., Baetz, B. W., Liu, L., Zhang, H., Fenech, A., & Liu, Z. (2018). Spatiotemporal Changes of China's Carbon Emissions. *Geophysical Research Letters*, 45(16), 8536–8546. <https://doi.org/10.1029/2018GL079564>
- Chen, C., Dubin, R., & Kim, M. C. (2014). Emerging trends and new developments in regenerative medicine: A scientometric update (2000 – 2014). *Expert Opinion on Biological Therapy*, 14(9), 1295–1317. <https://doi.org/10.1517/14712598.2014.920813>
- Chen, C., & Leydesdorff, L. (2014). Patterns of connections and movements in dual-map overlays: A new method of publication portfolio analysis. *Journal of the Association for Information Science and Technology*, 65(2), 334–351. <https://doi.org/10.1002/asi.22968>
- Chen, C., & Song, M. (2019). Visualizing a field of research: A methodology of systematic scientometric reviews. *PLOS ONE*, 14(10), e0223994. <https://doi.org/10.1371/journal.pone.0223994>
- Chen, M., Jia, W., Du, C., Shi, M., Henebry, G. M., & Wang, K. (2023). Carbon saving potential of urban parks due to heat mitigation in Yangtze River Economic Belt. *Journal of Cleaner Production*, 385, 135713. <https://doi.org/10.1016/j.jclepro.2022.135713>
- Chen, W. Y. (2015). *The role of urban green infrastructure in offsetting carbon emissions in 35 major Chinese cities: A nationwide estimate*. 9.
- Churkina, G., Brown, D. G., & Keoleian, G. (2010). Carbon stored in human settlements: The conterminous United States: CARBON IN HUMAN SETTLEMENTS. *Global Change Biology*, 16(1), 135–143. <https://doi.org/10.1111/j.1365-2486.2009.02002.x>
- Don, A., Seidel, F., Leifeld, J., Kätterer, T., Martin, M., Pellerin, S., Emde, D., Seitz, D., & Chenu, C. (2024). Carbon sequestration in soils and climate change mitigation—Definitions and pitfalls. *Global Change Biology*, 30(1), e16983. <https://doi.org/10.1111/gcb.16983>
- Ernst, F. B., Karabulut, A. İ., & Yeşilnacar, M. İ. (2022). Geodesign – a New Approach for Rapid Development of Planning and Carbon Sequestration Scenarios. In M. Ben Ahmed, A. A. Boudhir, İ. R. Karaş, V. Jain, & S. Mellouli (Eds.), *Innovations in Smart Cities Applications Volume 5* (pp. 559–570). Springer International Publishing. https://doi.org/10.1007/978-3-030-94191-8_45

Escobedo, F., Varela, S., Zhao, M., Wagner, J. E., & Zipperer, W. (2010). Analyzing the efficacy of subtropical urban forests in offsetting carbon emissions from cities. *Environmental Science & Policy*, 13(5), 362–372. <https://doi.org/10.1016/j.envsci.2010.03.009>

Falster, D. S., Duursma, R. A., Ishihara, M. I., Barneche, D. R., FitzJohn, R. G., Vårhammar, A., Aiba, M., Ando, M., Anten, N., Aspinwall, M. J., Baltzer, J. L., Baraloto, C., Battaglia, M., Battles, J. J., Bond-Lamberty, B., van Breugel, M., Camac, J., Claveau, Y., Coll, L., ... York, R. A. (2015). BAAD: A Biomass And Allometry Database for woody plants. *Ecology*, 96(5), 1445–1445. <https://doi.org/10.1890/14-1889.1>

Friedlingstein, P. (2015). Carbon cycle feedbacks and future climate change. *Philosophical Transactions of the Royal Society A: Mathematical, Physical and Engineering Sciences*, 373(2054), 20140421. <https://doi.org/10.1098/rsta.2014.0421>

Ge, S., & Zhao, S. (2017). Organic carbon storage change in China's urban landfills from 1978–2014. *Environmental Research Letters*, 12(10), 104013. <https://doi.org/10.1088/1748-9326/aa81df>

Guan, D., Nie, J., Zhou, L., Chang, Q., & Cao, J. (2023). How to Simulate Carbon Sequestration Potential of Forest Vegetation? A Forest Carbon Sequestration Model across a Typical Mountain City in China. *Remote Sensing*, 15(21), Article 21. <https://doi.org/10.3390/rs15215096>

Guan, Y., Shan, Y., Huang, Q., Chen, H., Wang, D., & Hubacek, K. (2021). Assessment to China's Recent Emission Pattern Shifts. *Earth's Future*, 9(11), e2021EF002241. <https://doi.org/10.1029/2021EF002241>

Guo, Q., Lai, X., Jia, Y., & Wei, F. (2023). Spatiotemporal Pattern and Driving Factors of Carbon Emissions in Guangxi Based on Geographic Detectors. *Sustainability*, 15(21), Article 21. <https://doi.org/10.3390/su152115477>

He, C., Liu, Z., Wu, J., Pan, X., Fang, Z., Li, J., & Bryan, B. A. (2021). Future global urban water scarcity and potential solutions. *Nature Communications*, 12(1), 4667. <https://doi.org/10.1038/s41467-021-25026-3>

Hong, W., Ren, Z., Guo, Y., Wang, C., Cao, F., Zhang, P., Hong, S., & Ma, Z. (2024). Spatiotemporal changes in urban forest carbon sequestration capacity and its potential drivers in an urban agglomeration: Implications for urban CO₂ emission mitigation under China's rapid

urbanization. *Ecological Indicators*, 159, 111601.
<https://doi.org/10.1016/j.ecolind.2024.111601>

Hou, J., Yang, X., & Chen, C. (2018). Emerging trends and new developments in information science: A document co-citation analysis (2009–2016). *Scientometrics*, 115(2), 869–892.
<https://doi.org/10.1007/s11192-018-2695-9>

Houghton, R. A. (2005). Aboveground Forest Biomass and the Global Carbon Balance. *Global Change Biology*, 11(6), 945–958. <https://doi.org/10.1111/j.1365-2486.2005.00955.x>

Hua, L. (2013). Linking landscape patterns with ecological functions: A case study examining the interaction between landscape heterogeneity and carbon stock of urban forests in Xiamen, China. *Forest Ecology and Management*, 293, 122–131.
<https://doi.org/10.1016/j.foreco.2012.12.043>

Jacquet, J., & Jamieson, D. (2016). Soft but significant power in the Paris Agreement. *Nature Climate Change*, 6(7), Article 7. <https://doi.org/10.1038/nclimate3006>

Janssens, I. A., Freibauer, A., Ciais, P., Smith, P., Nabuurs, G.-J., Folberth, G., Schlamadinger, B., Hutjes, R. W. A., Ceulemans, R., Schulze, E.-D., Valentini, R., & Dolman, A. J. (2003). Europe's Terrestrial Biosphere Absorbs 7 to 12% of European Anthropogenic CO₂ Emissions. *Science*, 300(5625), 1538–1542. <https://doi.org/10.1126/science.1083592>

Jia, X., Han, H., Feng, Y., Song, P., He, R., Liu, Y., Wang, P., Zhang, K., Du, C., Ge, S., & Tian, G. (2023). Scale-dependent and driving relationships between spatial features and carbon storage and sequestration in an urban park of Zhengzhou, China. *Science of The Total Environment*, 894, 164916. <https://doi.org/10.1016/j.scitotenv.2023.164916>

Jo, H.-K., Park, H.-M., & Kim, J.-Y. (2023). Carbon Offset Service of Urban Park Trees and Desirable Planting Strategies for Several Metropolitan Cities in South Korea. *Forests*, 14(2), 278. <https://doi.org/10.3390/f14020278>

Keller, D. P., Lenton, A., Littleton, E. W., Oshlies, A., Scott, V., & Vaughan, N. E. (2018). The Effects of Carbon Dioxide Removal on the Carbon Cycle. *Current Climate Change Reports*, 4(3), 250–265. <https://doi.org/10.1007/s40641-018-0104-3>

Kovalskyy, V., & Roy, D. P. (2013). The global availability of Landsat 5 TM and Landsat 7 ETM + land surface observations and implications for global 30 m Landsat data product generation. *REMOTE SENSING OF ENVIRONMENT*, 130, 280–293.

<https://doi.org/10.1016/j.rse.2012.12.003>

KS Mcgarigal, SA Cushman, MC Neel, & E Ene. (2002). *FRAGSTATS: Spatial pattern analysis program for categorical maps*.

http://www.researchgate.net/publication/259011515_FRAGSTATS_Spatial_pattern_analysis_program_for_categorical_maps

Kumar, M., Mukherjee, N., Sharma, G. P., & Raghubanshi, A. S. (2010). Land use patterns and urbanization in the holy city of Varanasi, India: A scenario. *Environmental Monitoring and Assessment*, 167(1–4), 417–422. <https://doi.org/10.1007/s10661-009-1060-0>

Lal, R. (2005). Forest soils and carbon sequestration. *Forest Ecology and Management*, 220(1–3), 242–258. <https://doi.org/10.1016/j.foreco.2005.08.015>

Lal, R. (2008). Carbon sequestration. *Philosophical Transactions of the Royal Society B: Biological Sciences*, 363(1492), 815–830. <https://doi.org/10.1098/rstb.2007.2185>

Li, X., Ma, H., Ran, Y., Wang, X., Zhu, G., Liu, F., He, H., Zhang, Z., & Huang, C. (2021). Terrestrial carbon cycle model-data fusion: Progress and challenges. *Science China Earth Sciences*, 64(10), 1645–1657. <https://doi.org/10.1007/s11430-020-9800-3>

Lin, J., Guo, Y., Li, J., Shao, M., & Yao, P. (2023). Spatial and temporal characteristics of carbon emission and sequestration of terrestrial ecosystems and their driving factors in mainland China—A case study of 352 prefectural administrative districts. *Frontiers in Ecology and Evolution*, 11. <https://doi.org/10.3389/fevo.2023.1169427>

Liu, C., & Li, X. (2012). Carbon storage and sequestration by urban forests in Shenyang, China. *Urban Forestry & Urban Greening*, 11(2), 121–128. <https://doi.org/10.1016/j.ufug.2011.03.002>

Lu, W., Liu, Z., Huang, Y., Bu, Y., Li, X., & Cheng, Q. (2020). How do authors select keywords? A preliminary study of author keyword selection behavior. *Journal of Informetrics*, 14(4), 101066. <https://doi.org/10.1016/j.joi.2020.101066>

Maheen, R., Cai, L., Zhang, Y. S., & Zhao, M. (2023). Quantitative analysis of carbon dioxide emission reduction pathways: Towards carbon neutrality in China's power sector. *Carbon Capture Science & Technology*, 7, 100112. <https://doi.org/10.1016/j.ccst.2023.100112>

McIntyre, N. E., Knowles-Yáñez, K., & Hope, D. (2008). Urban Ecology as an Interdisciplinary Field: Differences in the use of “Urban” Between the Social and Natural Sciences. In J. M.

- Marzluff, E. Shulenberger, W. Endlicher, M. Alberti, G. Bradley, C. Ryan, U. Simon, & C. ZumBrunnen (Eds.), *Urban Ecology* (pp. 49–65). Springer US. https://doi.org/10.1007/978-0-387-73412-5_4
- Meng, Y., Gou, R., Bai, J., Moreno-Mateos, D., Davis, C. C., Wan, L., Song, S., Zhang, H., Zhu, X., & Lin, G. (2022). Spatial patterns and driving factors of carbon stocks in mangrove forests on Hainan Island, China. *Global Ecology and Biogeography*, 31(9), 1692–1706. <https://doi.org/10.1111/geb.13549>
- Nor Akmar, A. A., Konijnendijk, C. C., Sreetheran, M., & Nilsson, K. (2011). Greenspace Planning and Management in Klang Valley, Peninsular Malaysia. *Arboriculture & Urban Forestry*, 37(3), 99–107. <https://doi.org/10.48044/jauf.2011.014>
- Nowak, D. J., & Crane, D. E. (2002). Carbon storage and sequestration by urban trees in the USA. *Environmental Pollution*, 116(3), 381–389. [https://doi.org/10.1016/S0269-7491\(01\)00214-7](https://doi.org/10.1016/S0269-7491(01)00214-7)
- Pacala, S. W., Hurtt, G. C., Baker, D., Peylin, P., Houghton, R. A., Birdsey, R. A., Heath, L., Sundquist, E. T., Stallard, R. F., Ciais, P., Moorcroft, P., Caspersen, J. P., Shevliakova, E., Moore, B., Kohlmaier, G., Holland, E., Gloor, M., Harmon, M. E., Fan, S.-M., ... Field, C. B. (2001). Consistent Land- and Atmosphere-Based U.S. Carbon Sink Estimates. *Science*, 292(5525), 2316–2320. <https://doi.org/10.1126/science.1057320>
- Raum, S., Hand, K. L., Hall, C., Edwards, D. M., O'Brien, L., & Doick, K. J. (2019). Achieving impact from ecosystem assessment and valuation of urban greenspace: The case of i-Tree Eco in Great Britain. *Landscape and Urban Planning*, 190, 103590. <https://doi.org/10.1016/j.landurbplan.2019.103590>
- Reichstein, M., Bahn, M., Ciais, P., Frank, D., Mahecha, M. D., Seneviratne, S. I., Zscheischler, J., Beer, C., Buchmann, N., Frank, D. C., Papale, D., Rammig, A., Smith, P., Thonicke, K., Van Der Velde, M., Vicca, S., Walz, A., & Wattenbach, M. (2013). Climate extremes and the carbon cycle. *Nature*, 500(7462), 287–295. <https://doi.org/10.1038/nature12350>
- Sabe, M., Pillinger, T., Kaiser, S., Chen, C., Taipale, H., Tanskanen, A., Tiuhonen, J., Leucht, S., Correll, C. U., & Solmi, M. (2022). Half a century of research on antipsychotics and schizophrenia: A scientometric study of hotspots, nodes, bursts, and trends. *Neuroscience & Biobehavioral Reviews*, 136, 104608. <https://doi.org/10.1016/j.neubiorev.2022.104608>

Schomaker, M. E., Zarnoch, S. J., Bechtold, W. A., Latelle, D. J., Burkman, W. G., & Cox, S. M. (2007). *Crown-condition classification: A guide to data collection and analysis* (SRS-GTR-102; p. SRS-GTR-102). U.S. Department of Agriculture, Forest Service, Southern Research Station. <https://doi.org/10.2737/SRS-GTR-102>

Shadman, S., Ahanaf Khalid, P., Hanafiah, M. M., Koyande, A. K., Islam, Md. A., Bhuiyan, S. A., Sin Woon, K., & Show, P.-L. (2022). The carbon sequestration potential of urban public parks of densely populated cities to improve environmental sustainability. *Sustainable Energy Technologies and Assessments*, 52, 102064. <https://doi.org/10.1016/j.seta.2022.102064>

Shan, Y., Guan, D., Zheng, H., Ou, J., Li, Y., Meng, J., Mi, Z., Liu, Z., & Zhang, Q. (2018). China CO₂ emission accounts 1997–2015. *Scientific Data*, 5(1), 170201. <https://doi.org/10.1038/sdata.2017.201>

Shan, Y., Huang, Q., Guan, D., & Hubacek, K. (2020). China CO₂ emission accounts 2016–2017. *Scientific Data*, 7(1), 54. <https://doi.org/10.1038/s41597-020-0393-y>

Shang, M., & Luo, J. (2021). The Tapio Decoupling Principle and Key Strategies for Changing Factors of Chinese Urban Carbon Footprint Based on Cloud Computing. *International Journal of Environmental Research and Public Health*, 18(4), Article 4. <https://doi.org/10.3390/ijerph18042101>

Shi, M., Wu, H., Jiang, P., Shi, W., Zhang, M., Zhang, L., Zhang, H., Fan, X., Liu, Z., Zheng, K., Dong, T., & Baqa, M. F. (2022). Cropland Expansion Mitigates the Supply and Demand Deficit for Carbon Sequestration Service under Different Scenarios in the Future—The Case of Xinjiang. *Agriculture*, 12(8), Article 8. <https://doi.org/10.3390/agriculture12081182>

Shi, N., Yu, Y., Liang, S., Ren, Y., & Liu, M. (2024). Effects of urban green spaces landscape pattern on carbon sink among urban ecological function areas at the appropriate scale: A case study in Xi'an. *Ecological Indicators*, 158, 111427. <https://doi.org/10.1016/j.ecolind.2023.111427>

Silaydin Aydin, M. B., & Çukur, D. (2012). Maintaining the carbon–oxygen balance in residential areas: A method proposal for land use planning. *Urban Forestry & Urban Greening*, 11(1), 87–94. <https://doi.org/10.1016/j.ufug.2011.09.008>

Song, J., Zhang, R., Wang, Y., & Huang, J. (2023). Evolution Characteristics of Wetland Landscape Pattern and Its Impact on Carbon Sequestration in Wuhan from 2000 to 2020. *Land*,

12(3), 582. <https://doi.org/10.3390/land12030582>

Sun, Y., Xie, S., & Zhao, S. (2019). Valuing urban green spaces in mitigating climate change: A city-wide estimate of aboveground carbon stored in urban green spaces of China's Capital. *Global Change Biology*, 25(5), 1717–1732. <https://doi.org/10.1111/gcb.14566>

Tang, Z., Wang, Y., Fu, M., & Xue, J. (2023). The role of land use landscape patterns in the carbon emission reduction: Empirical evidence from China. *Ecological Indicators*, 156, 111176. <https://doi.org/10.1016/j.ecolind.2023.111176>

Van Der Werf, G. R., Morton, D. C., DeFries, R. S., Olivier, J. G. J., Kasibhatla, P. S., Jackson, R. B., Collatz, G. J., & Randerson, J. T. (2009). CO₂ emissions from forest loss. *Nature Geoscience*, 2(11), 737–738. <https://doi.org/10.1038/ngeo671>

Wang, D., Wang, B., & Niu, X. (2014). Forest carbon sequestration in China and its benefits. *Scandinavian Journal of Forest Research*, 29(1), 51–59. <https://doi.org/10.1080/02827581.2013.856936>

Wang, Y., Chang, Q., & Li, X. (2021). Promoting sustainable carbon sequestration of plants in urban greenspace by planting design: A case study in parks of Beijing. *Urban Forestry & Urban Greening*, 64, 127291. <https://doi.org/10.1016/j.ufug.2021.127291>

Weissert, L. F., Salmond, J. A., & Schwendenmann, L. (2017). Photosynthetic CO₂ uptake and carbon sequestration potential of deciduous and evergreen tree species in an urban environment. *Urban Ecosystems*, 20(3), 663–674. <https://doi.org/10.1007/s11252-016-0627-0>

Williams, N., Hahs, A. K., & Vesk, P. A. (2015). Urbanisation, plant traits and the composition of urban floras. *Perspectives in Plant Ecology Evolution & Systematics*, 17(1), Article 1. <https://doi.org/10.1016/j.ppees.2014.10.002>

Xu, F., Wang, X., & Li, L. (2023). NPP and Vegetation Carbon Sink Capacity Estimation of Urban Green Space Using the Optimized CASA Model: A Case Study of Five Chinese Cities. *Atmosphere*, 14(7), 1161. <https://doi.org/10.3390/atmos14071161>

Xu, M., He, C., Liu, Z., & Dou, Y. (2016). How Did Urban Land Expand in China between 1992 and 2015? A Multi-Scale Landscape Analysis. *PLOS ONE*, 11(5), e0154839. <https://doi.org/10.1371/journal.pone.0154839>

Yin, S., Wang, J., & Zeng, H. (2023). A bibliometric study on carbon cycling in vegetated blue

carbon ecosystems. *Environmental Science and Pollution Research*, 30(30), 74691–74708.
<https://doi.org/10.1007/s11356-023-27816-2>

Yokohari, M., & Bolthouse, J. (2011). Planning for the slow lane: The need to restore working greenspaces in maturing contexts. *Landscape and Urban Planning*, 100(4), 421–424.
<https://doi.org/10.1016/j.landurbplan.2011.02.024>

Zhang, W., Huang, B., & Luo, D. (2014). Effects of land use and transportation on carbon sources and carbon sinks: A case study in Shenzhen, China. *Landscape and Urban Planning*, 122, 175–185. <https://doi.org/10.1016/j.landurbplan.2013.09.014>

Zhao, J., Ouyang, Z., Xu, W., Zheng, H., & Meng, X. (2010). Sampling adequacy estimation for plant species composition by accumulation curves—A case study of urban vegetation in Beijing, China. *Landscape and Urban Planning*, 95(3), 113–121.
<https://doi.org/10.1016/j.landurbplan.2009.12.008>

Zhao, Y., Su, Q., Li, B., Zhang, Y., Wang, X., Zhao, H., & Guo, S. (2022). Have those countries declaring “zero carbon” or “carbon neutral” climate goals achieved carbon emissions-economic growth decoupling? *Journal of Cleaner Production*, 363, 132450.
<https://doi.org/10.1016/j.jclepro.2022.132450>

Zhou, Q., Liao, Y., & Wang, J. (2022). Mapping global urban greenspace: An analysis based on open land-cover data. *Urban Forestry & Urban Greening*, 74, 127638.
<https://doi.org/10.1016/j.ufug.2022.127638>

Zhou, Y., Tu, M., Wang, S., & Liu, W. (2018). A Novel Approach for Identifying Urban Built-Up Area Boundaries Using High-Resolution Remote-Sensing Data Based on the Scale Effect. *ISPRS International Journal of Geo-Information*, 7(4), Article 4. <https://doi.org/10.3390/ijgi7040135>

Zhu, Z. (2019). Science of Landsat Analysis Ready Data. *Remote Sensing*, 11(18), Article 18.
<https://doi.org/10.3390/rs11182166>

Appendix

Vegetable Field Research Sheet

Sheet _____ of _____

[illegible]

Appendix 1 On-site Research Statistical Table

Appendix 2 Remote sensing data description

| Year | Image ID | Year | Image ID | Year | Image ID |
|------|-------------------|------|-------------------|------|-------------------|
| 2013 | #_124035_20130331 | 2018 | #_124035_20180314 | 2023 | #_125035_20230303 |
| | #_124035_20130410 | | #_124036_20180314 | | #_125036_20230303 |
| | #_124036_20130410 | | #_124036_20180314 | | #_123036_20230305 |
| | #_124037_20130410 | | #_124036_20180314 | | #_123037_20230305 |
| | #_124035_20130417 | | #_124036_20180314 | | #_124035_20230312 |
| | #_125035_20130424 | | #_123037_20180323 | | #_124036_20230312 |
| | #_125036_20130424 | | #_124035_20180330 | | #_125035_20230319 |
| | #_123036_20130426 | | #_124036_20180330 | | #_124035_20230328 |
| | #_123037_20130426 | | #_124037_20180330 | | #_124036_20230328 |
| | #_124035_20130503 | | #_125036_20180406 | | #_125035_20230420 |
| | #_124036_20130503 | | #_123036_20180408 | | #_125036_20230420 |
| | #_124037_20130503 | | #_123037_20180408 | | #_124035_20230429 |
| | #_123036_20130512 | | #_124035_20180415 | | #_124036_20230429 |
| | #_123037_20130512 | | #_124036_20180415 | | #_124037_20230429 |
| | #_124035_20130519 | | #_125035_20180508 | | #_123036_20230508 |
| | #_124035_20130604 | | #_125036_20180508 | | #_124035_20230515 |
| | #_124036_20130604 | | #_123036_20180510 | | #_124036_20230515 |
| | #_124037_20130604 | | #_123037_20180510 | | #_124037_20230515 |
| | #_125035_20130611 | | #_123036_20180526 | | #_125035_20230522 |
| | #_125036_20130611 | | #_123036_20180611 | | #_125036_20230522 |
| | #_123036_20130613 | | #_123037_20180611 | | #_123036_20230524 |
| | #_123037_20130613 | | #_124035_20180720 | | #_123036_20230609 |
| | #_125035_20130627 | | #_124036_20180720 | | #_123037_20230609 |
| | #_125036_20130627 | | #_124037_20180720 | | #_125035_20230623 |
| | #_124035_20130706 | | #_125035_20180727 | | #_125036_20230623 |
| | #_124036_20130706 | | #_125035_20180812 | | #_125035_20230709 |
| | #_124037_20130706 | | #_125036_20180812 | | #_125036_20230709 |
| | #_123036_20130731 | | #_124035_20180821 | | #_123036_20230711 |
| | #_123037_20130731 | | #_124036_20180821 | | #_123037_20230711 |
| | #_124035_20130807 | | #_124037_20180821 | | #_124035_20230718 |

| | | |
|-------------------|-------------------|-------------------|
| #_124036_20130807 | #_125035_20180828 | #_124036_20230718 |
| #_124037_20130807 | #_125036_20180828 | #_124037_20230718 |
| #_125035_20130814 | #_123037_20180830 | #_125035_20230725 |
| #_125036_20130814 | #_124035_20180906 | #_125036_20230725 |
| #_123036_20130816 | #_124035_20180922 | #_123036_20230727 |
| #_123037_20130816 | #_124036_20180922 | #_124035_20230803 |
| #_124035_20130823 | #_124037_20180922 | #_124036_20230803 |
| #_125035_20130830 | #_125035_20180929 | #_124037_20230803 |
| #_125036_20130830 | #_125036_20180929 | #_125035_20230810 |
| #_123036_20130901 | #_123036_20181001 | #_125036_20230810 |
| #_123037_20130901 | #_123037_20181001 | #_123037_20230812 |
| #_125036_20130915 | #_124035_20181008 | #_123036_20230828 |
| #_123036_20130917 | #_125035_20181015 | #_124035_20230904 |
| #_123037_20130917 | #_125036_20181015 | #_124036_20230904 |
| #_123036_20131003 | #_123036_20181017 | #_124037_20230904 |
| #_123037_20131003 | #_123037_20181017 | #_123036_20230913 |
| #_124035_20131010 | #_124035_20181024 | #_124035_20230920 |
| #_124036_20131010 | #_124036_20181024 | #_124036_20230920 |
| #_124037_20131010 | #_124037_20181024 | #_125035_20231013 |
| #_125035_20131017 | | #_125036_20231013 |
| | | #_123036_20231015 |
| | | #_123037_20231015 |
| | | #_124035_20231022 |
| | | #_124036_20231022 |
| | | #_124037_20231022 |
| | | #_125035_20231029 |
| | | #_125036_20231029 |

represent LANDSAT/LC08/C02/T1_L2/LC08

Appendix 3 Biomass allometric equations of different species

| Shrub species | Biomass equation (kg) | a | b | c | R ² | P |
|-----------------------------------------------------------|-------------------------------------------------------------------------|----------|---------|-------------|----------------|--------|
| <i>Rhus chinensis</i> Mill. | $W_T = a(D^2 \cdot H)^b$ | 1.205 | 0.673 | | 0.929 | <0.001 |
| <i>Lindera aggregata</i> (Sims) Kosterm. | $W_T = a(D^2 \cdot H)^b$ | 0.632 | 0.858 | | 0.961 | <0.001 |
| <i>Ardisia crenata</i> Sims | $W_T = a \cdot (D^2 \cdot H)^2 + b \cdot (D^2 \cdot H) + c$ | -0.00022 | 0.423 | 4.517 | 0.87 | <0.001 |
| <i>Lindera glauca</i> (Siebold & Zucc.) Blume | $W_T = a \cdot D^b$ | 55.176 | 1.941 | | 0.865 | <0.001 |
| <i>Amorpha fruticosa</i> | $W_T = a + b \cdot H + c \cdot H^2$ | -0.285 | 0.785 | -0.18 | 0.945 | <0.001 |
| <i>Lespedeza bicolor</i> | $W_T = a + b \cdot H + c \cdot H^2$ | -0.055 | 0.135 | 0.06 | 0.955 | <0.001 |
| <i>Vitex negundo</i> | $W_T = a + b \cdot H + c \cdot H^2$ | 0.213 | -0.075 | 0.154 | 0.952 | <0.001 |
| <i>Caragana microphylla</i> | $W_T = a \cdot C^b$ | 0.82 | 0.82 | | 0.86 | <0.001 |
| <i>Salix gordejewii</i> | $W_T = a \cdot \ln C + b$ | 2.08 | 1.07 | | 0.8 | <0.001 |
| <i>Caragana korshinskii</i> | $W_T = a + b \cdot (C^2 \cdot H/4) + c \cdot (C^2 \cdot H/4)^2$ | 0.08 | 0.453 | -0.005 | 0.6 | <0.001 |
| <i>Hippophae rhamnoides</i> | $W_T = a(D^2 \cdot H)^b$ | 0.103 | 0.838 | | 0.94 | <0.001 |
| <i>Salix cheilophila</i> | $W_T = a + b \cdot (C^2 \cdot H/4)$ | 0.547 | 0.399 | | 0.8 | <0.001 |
| <i>Corethroedendron fruticosum</i> var. <i>mongolicum</i> | $W_T = a + b \cdot (C^2 \cdot H/4) + c \cdot (C^2 \cdot H/4)^2$ | 0.054 | 0.123 | 0.041 | 0.7 | <0.001 |
| <i>Reaumuria songarica</i> | $W_T = a + b \cdot (C^2 \cdot H/4) + c \cdot (C^2 \cdot H/4)^2$ | 17.884 | 0.0062 | -0.00000004 | 0.909 | <0.001 |
| <i>Sympegma regelii</i> Bunge | $W_T = a + b \cdot ((C/2)^2 \cdot \pi) + c \cdot ((C/2)^2 \cdot \pi)^2$ | -0.849 | 0.0166 | 0.000004 | 0.935 | <0.001 |
| <i>Gymnocarpus przewalskii</i> Maxim. | $W_T = a(((C/2)^2 \cdot \pi))^b$ | 1.12 | 499.63 | | 0.6 | <0.001 |
| <i>Prunus mongolica</i> Maxim. | $W_T = a(((C/2)^2 \cdot \pi) \cdot H)^b$ | 1.04 | 955.57 | | 0.89 | <0.001 |
| <i>Spiraea lasiocarpa</i> | $W_T = a(((C/2)^2 \cdot \pi) \cdot H)^b$ | 1.28 | 1437.99 | | 0.87 | <0.001 |
| <i>Potaninia mongolica</i> | $W_T = a(((C/2)^2 \cdot \pi) \cdot H) + b$ | 1323.1 | 4.13 | | 0.85 | <0.001 |
| <i>Ephedra przewalskii</i> Stapf | $W_T = a \cdot H + b \cdot ((C/2)^2 \cdot \pi) + c$ | 22.64 | 823.21 | 5.52 | 0.84 | <0.001 |

| | | | | | | |
|---------------------------|-----------------------------------------------------------------------------------|---------|---------|----------|-------|--------|
| Nitraria sphaerocarpa | $W_T=a(((C/2)^2 \cdot \pi) \cdot H)+b$ | 775.85 | 16.66 | | 0.63 | <0.001 |
| Ammopiptanthus mongolicus | $W_T=a(((C/2)^2 \cdot \pi))^b$ | 1 | 721.94 | | 0.92 | <0.001 |
| Salix psammophila | $W_T=a(((C/2)^2 \cdot \pi) \cdot H)^b$ | 0.73 | 261.44 | | 0.66 | <0.001 |
| Tetraena mongolica | $W_T=a(((C/2)^2 \cdot \pi))^b$ | 1.11 | 665.12 | | 0.82 | <0.001 |
| Haloxylon ammodendron | $W_T=a(((C/2)^2 \cdot \pi))^b$ | 1.29 | 1742.76 | | 0.82 | <0.001 |
| Indigofera bungeana | $W_T=a(((C/2)^2 \cdot \pi) \cdot H)+b$ | 1103.55 | 2.93 | | 0.92 | <0.001 |
| Spiraea pubescens | $W_T=a(((C/2)^2 \cdot \pi) \cdot H)^b$ | 0.86 | 878.75 | | 0.74 | <0.001 |
| Prunus sibirica | $W_T=a(((C/2)^2 \cdot \pi) \cdot H)+b$ | 599.33 | 14.12 | | 0.91 | <0.001 |
| Caragana stenophylla | $W_T=a(((C/2)^2 \cdot \pi))^b$ | 1.07 | 159.39 | | 0.55 | <0.001 |
| Forsythia suspensa | $W=a+b(D^2 \cdot H)+c(D^2 \cdot H)^3$ | 220.538 | 154.166 | 1.491 | 0.807 | <0.001 |
| Rosa xanthina | $W=a+b \cdot ((C/2)^2 \cdot \pi) \cdot H+c \cdot (((C/2)^2 \cdot \pi) \cdot H)^2$ | 277.428 | 0.001 | 8.73E-10 | 0.755 | <0.001 |
| Ostryopsis davidiana | $W=a \cdot D^b$ | 0.54 | 1.29 | | 0.89 | <0.001 |
| Syringa oblata | $W=a \cdot e^{b \cdot D \cdot D \cdot H}$ | 151.36 | 0.01 | | 0.82 | <0.001 |
| Rhamnus parvifolia Bunge | $W=a \cdot (D^2 \cdot H)^b$ | 12.616 | 0.535 | | 0.742 | <0.001 |
| Syringa pubescens | $W=a \cdot (D^2 \cdot H)^b$ | 10.26 | 0.55 | | 0.802 | <0.001 |
| Fraxinus chinensis | $W=a \cdot (D^2 \cdot H)^b$ | 7.283 | 0.622 | | 0.683 | <0.001 |
| Ulmus macrocarpa Hance | $W=a \cdot (D^2 \cdot H)^b$ | 15.384 | 0.46 | | 0.782 | <0.001 |
| Spiraea trilobata | $W=a \cdot (D^2 \cdot H)^b$ | 18.516 | 0.774 | | 0.679 | <0.001 |

DECLARATION

the public access and authenticity of the thesis

Student's name: FENG YUAN

Student's Neptun code: PVBTLF

Title of thesis: Changes in Carbon Sequestration Capacity of Urban Green Spaces and Optimization Pathways -- a case study of Zhengzhou Metropolitan Area

Year of publication: 2024

Name of the consultant's institute: Institute of Landscape Architecture

Name of consultant's department: Department of Landscape Planning and Regional Development

I declare that the final thesis/thesis/dissertation/portfolio submitted by me is an individual, original work of my own intellectual creation. I have clearly indicated the parts of my thesis or dissertation which I have taken from other authors' work and have included them in the bibliography.

If the above statement is untrue, I understand that I will be disqualified from the final examination by the final examination board and that I will have to take the final examination after writing a new thesis.

I do not allow editing of the submitted thesis, but I allow the viewing and printing, which is a PDF document.

I acknowledge that the use and exploitation of my thesis as an intellectual work is governed by the intellectual property management regulations of the Hungarian University of Agricultural and Life Sciences.

I acknowledge that the electronic version of my thesis will be uploaded to the library repository of the Hungarian University of Agricultural and Life Sciences. I acknowledge that the defended and

- not confidential thesis after the defence
- confidential thesis 5 years after the submission

will be available publicly and can be searched in the repository system of the University.

Date: 2024 year 4 month 28 day

FENG YUAN

Student's signature

DECLARATION

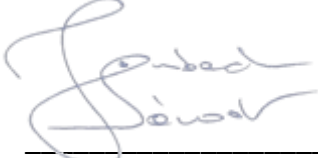
Feng Yuan (name) (student Neptun code: _PVBTLF_)

as a consultant, I declare that I have reviewed the final thesis/thesis/dissertation/portfolio¹ and that I have informed the student of the requirements, legal and ethical rules for the correct handling of literary sources.

I recommend / do not recommend² the final thesis / dissertation / portfolio to be defended in the final examination.

The thesis contains a state or official secret: yes no^{*3}

Date: 2024 year April month 29 day



insider consultant

¹ The other types should be deleted while retaining the corresponding thesis type.

² The appropriate one should be underlined.

³ The appropriate one should be underlined.